On the Formation of a Subsurface Weakly Sheared Laminar Layer and an Upper Thermocline Strongly Sheared Turbulent Layer in the Eastern Equatorial Pacific: Interplays of Multiple-Time-Scale Equatorial Waves

CHUANYU LIU AND XIAOWEI WANG

CAS Key Laboratory of Ocean Circulation and Waves, Institute of Oceanology, Chinese Academy of Sciences, and Marine Dynamic Process and Climate Function Laboratory, Pilot National Laboratory for Marine Science and Technology (Qingdao), and Center for Ocean Mega-Science, Chinese Academy of Sciences, Qingdao, and University of the Chinese Academy of Sciences, Beijing, China

ZHIYU LIU

State Key Laboratory of Marine Environmental Science, and Department of Physical Oceanography, College of Ocean and Earth Sciences, Xiamen University, Xiamen, China

ARMIN KÖHL

Institute of Oceanography, University of Hamburg, Hamburg, Germany

WILLIAM D. SMYTH

College of Earth, Ocean and Atmospheric Sciences, Oregon State University, Corvallis, Oregon

FAN WANG

CAS Key Laboratory of Ocean Circulation and Waves, Institute of Oceanology, Chinese Academy of Sciences, and Marine Dynamic Process and Climate Function Laboratory, Pilot National Laboratory for Marine Science and Technology (Qingdao), and Center for Ocean Mega-Science, Chinese Academy of Sciences, Qingdao, and University of the Chinese Academy of Sciences, Beijing, China

(Manuscript received 16 October 2019, in final form 10 July 2020)

ABSTRACT

The origins of an observed weakly sheared nonturbulent (laminar) layer (WSL), and a strongly sheared turbulent layer above the Equatorial Undercurrent core (UCL) in the eastern equatorial Pacific are studied, based mainly on the data from the Tropical Atmosphere and Ocean mooring array. Multiple-time-scale (from 3 to 25 days) equatorial waves were manifested primarily as zonal velocity oscillations with the maximum amplitudes (from 10 to 30 cm s⁻¹) occurring at different depths (from the surface to 85-m depths) above the seasonal thermocline. The subsurface-intensified waves led to vertically out-of-phase shear variations in the upper thermocline via destructive interference with the seasonal zonal flow, opposing the tendency for shear instability. These waves were also associated with depth-dependent, multiple-vertical-scale stratification variations, with phase lags of $\pi/2$ or π , further altering stability of the zonal current system to vertical shear. The WSL and UCL were consequently formed by coupling of multiple equatorial waves with differing phases, particularly of the previously identified equatorial mode and subsurface mode tropical instability waves (with central period of 17 and 20 days, respectively, in this study), and subsurface-intensified waves with central periods of 6, 5, and 12 days and velocity maxima at 45-, 87-, and 40-m depths, respectively. In addition, a wave-like feature with periods of 50–90 days enhanced the shear throughout the entire UCL. WSLs and UCLs seem

Openotes content that is immediately available upon publication as open access.

Corresponding author: Chuanyu Liu, chuanyu.liu@qdio.ac.cn

DOI: 10.1175/JPO-D-19-0245.1

to emerge without a preference for particular tropical instability wave phases. The generation mechanisms of the equatorial waves and their joint impacts on thermocline mixing remain to be elucidated.

1. Introduction

The surface mixed layer (ML) in the equatorial cold tongue of the central and eastern Pacific plays an important role in tropical atmosphere–ocean interactions. The thermal structure of the ML is governed by the balance of the cooling by the vertical turbulent heat flux at the base of the ML (~100 W m⁻²), surface warming (~70 W m⁻²), and meridional advection (~50 W m⁻²; Wang and McPhaden 1999, 2001), while the seasonal variation of the sea surface temperature is recognized to be controlled largely by the subsurface turbulent heat flux (Moum et al. 2013). The dynamics of turbulence herein has therefore attracted many research efforts.

Turbulence has been observed at 0°, 140°W (Eq140W hereafter), the main locus of ocean heat uptake, in several expeditions including Tropic Heat 1 (TH1, 1984; Gregg et al. 1985; Moum and Caldwell 1985), Tropic Heat 2 (TH2, 1987; Peters et al. 1991), the Tropical Instability Wave Experiment (TIWE, 1991; Lien et al. 1995), and the Equatorial Internal Wave Experiment (EQUIX, 2008; Moum et al. 2009, hereafter M09; Inoue et al. 2012, hereafter I12). These measurements revealed unique processes that determine the heat transport from the ML to the thermocline. In particular, TH1 revealed a deep-cycle layer (DCL) of turbulence at Eq140W: turbulence and internal wave activity were enhanced at night, extending below the surface ML into a stratified sheared layer of several tens of meters thick. Nighttime turbulent kinetic energy dissipation rate in the DCL exceeded the daytime value by more than an order of magnitude (Moum et al. 1992, 2011), and isotherm displacements and shear variances at nighttime were several times daytime levels (McPhaden and Peters 1992; Peters et al. 1994). The enhanced shear variance could penetrate into the upper thermocline. Subsequent studies showed that the DCL is an omnipresent feature at Eq140W, albeit with a distinct seasonal cycle (Pham et al. 2017). During 1-6 November 2008, EQUIX revealed an unusual layer of elevated shear and turbulence above the core of the Equatorial Undercurrent (EUC), which was named the upper core layer (UCL). The UCL appeared to be associated with the passage of a tropical instability wave (TIW). More interestingly, over much of this period, the DCL and the UCL were separated by a thin, weakly sheared, essentially nonturbulent (laminar) layer (M09; I12; referred to as WSL hereafter). The WSL was centered at ~50-m depth of about 10 m thickness during 4–7 November (which was separated from the WSL

at \sim 50–80 m on 1–2 November by a merged UCL–DCL turbulent layer on 3 November). The vertical penetration of strong shear variance below the base of the surface ML ended immediately above the WSL. The WSL appeared to be prominent during the southward (S) phase of the TIW. On the other hand, the UCL was immediately above the EUC core during the southward phase, with elevated zonal and meridional shears accompanied by strong turbulence. During the transition period from the northward to southward (N-S) phase and the early part of the S phase of the TIW, the UCL appeared to be merged with the DCL (at 50–100-m depth), and thus became indistinguishable; whereas, during the middle to late S phase, the UCL (at 70–100-m depth) was dynamically separated from the surface-driven DCL by the WSL. The WSL and UCL were not observed in the TH1, TH2, and TIWE experiments. (Readers may refer to Figs. 4 and 5 of I12 for a clear illustration of these distinct layers.)

The dynamics of the diurnal DCL, particularly from a perspective of its relationship to internal waves and shear instability, have been extensively studied both theoretically and numerically since TH1 (Boyd et al. 1993; Skyllingstad and Denbo 1994; Sutherland 1996; Mack and Hebert 1997; Sun et al. 1998; Wang et al. 1998; Wang and Müller 2002; Wijesekera and Dillon 1991; Moum et al. 1992; Lien et al. 1996; Mack and Hebert 1999; Smyth and Moum 2002; Pham et al. 2013, 2017). Two plausible formation mechanisms have been proposed. One suggested that internal waves generated at the base of the ML could transport momentum downward, adding small-scale shear into the already near-critical (i.e., marginally unstable) shear layer associated with the EUC, triggering shear instability (Moum and Caldwell 1985; Gregg et al. 1985; Wijesekera and Dillon 1991). The other argued that, rather than internal waves, turbulent entrainment immediately below the base of the ML transported momentum into the strong mean shear zone, enhancing shear and thus generating instability (Schudlich and Price 1992; Clayson and Kantha 1999; Smyth and Moum 2013, Smyth et al. 2013, 2017; Pham et al. 2013, 2017).

At the same time, less progress has been made on the dynamics of the UCL and WSL. Because the UCL and WSL were both observed during a TIW, they were naturally presumed to be a distinct feature associated with the TIW (I12). M09 attributed the enhanced mixing during the EQUIX experiment to the vertical shear associated with the TIW's meridional velocity. Holmes and Thomas (2015) found instead that the vertical shear

associated with the TIW's zonal velocity contributed most to the total vertical shear, and argued that the shear was caused by the meridional gradient of the TIWassociated meridional velocity via vortex stretching. Liu et al. (2019a) identified the northeast-southwestward (NE-SW) velocity oscillation of the equatorial mode TIW (eTIW hereafter), and argued that its westward velocity could induce strong vertical shear squared via its nonlinear interactions with the mean zonal flow (therein, "nonlinear interaction" means the jointly induced quadratic shear squared from linear superposition of their shears; whether the two processes indeed interacted in a common nonlinear sense or resulted in feedback to any of the processes was not considered). However, while these results seemed to have potential in explaining the existence of the UCL from the perspective of TIWs, the formation mechanism of the WSL, which blocked the DCL from penetrating further downward, remains unrevealed.

Recently, Liu et al. (2019b, hereafter L19b) discovered subsurface-intensified instability waves (named as subTIWs) at the equator that were mainly manifested as prominent zonal velocity oscillations. These waves had velocity amplitudes of 10–20 cm s⁻¹, peaked at 70–90-m depths, and were most significant during the commonly recognized TIW seasons which usually last for 3-7 months. It was found that the subTIWs could account for ~20% of the 5-30-day zonal velocity variance. L19b demonstrated that the shears associated with the subTIWs could lead to complex vertical structure of the shear squared (SS) changes (SSCs) above the EUC core. At certain phases, enhanced shear might occur just above the EUC core with weakened shear at ~50 m. The authors argued that this could explain the observed complex shear and mixing structures, including both the WSL and UCL, in the EQUIX experiment. However, the exact processes were not explored. Also not discussed was the joint effect of the subTIW with the more energetic, surface-intensified eTIW (contributing ~60% of the 5– 30-day variance). Finally, it was not known whether other kinds of waves also existed during the time period and how much they contributed to the shear and mixing.

In the present study, we extend the analysis of M09, I12, and L19b to describe the WSL and UCL in light of the interactions among the subTIW, the eTIW, the seasonal zonal flow, and other equatorial waves with different time scales and different depths of maximum amplitude. We will also examine whether the WSL and UCL can only occur at specific phases of TIWs. The data used for these analyses are described in section 2. In section 3, we propose the formation mechanisms, by first disclosing multiple-time-scale equatorial waves, and then demonstrating their interactions; we will also

demonstrate the existence of the two-layer structure during other TIWs. The conclusions and further discussions are presented in section 4.

2. Data and methods

In the present study, the observed hourly ocean temperature, salinity and velocity data at Eq140W are used. The data were collected by the Tropical Atmosphere and Ocean (TAO) mooring array (McPhaden 1995) and freely downloaded from http://www.pmel.noaa.gov/tao/ data_deliv. The velocity data have a vertical resolution of 5 m, while the temperature was measured at nonuniform vertical intervals, with an average interval of \sim 6 m above 80-m depth and ~12 m between 80- and 140-m depths. The original hourly salinity data are sparse and hence replaced by the long-time mean (Smyth and Moum 2013; Liu et al. 2016). All the data were interpolated and/or extrapolated into 1-m grids using a method described in detail by Liu et al. (2016). Hourly density profiles are calculated afterward. The time period for the analysis is September 2008–January 2009, with an emphasis on the period of intensive turbulence measurements of the EQUIX experiment (24 October-9 November 2008).

3. Results

a. TIWs and multiple-time-scale equatorial waves

To determine whether other kind of waves also existed during the time period of the EQUIX experiment, we conduct standard power spectral density (PSD) analysis on the hourly zonal and meridional velocity components (u and v, respectively) at each depth for a 4-month period (15 September 2008–15 January 2009). The Hanning window is adopted and its length is set as 90 days. The overlap length for two consecutive Hanning windows is 80 days, therefore in total five consecutive windows are used for the PSD calculation. The final PSD is an average over the five ensembles and the reported results are significant at 95% confidence level.

The calculated PSD is shown in Fig. 1. A variety of waves (wave continuums), manifested as PSD peaks at different depths with different periods in the *zonal* velocity component, are distinguishable above the thermocline center (Figs. 1a,b). Specifically, seven waves can be loosely picked up, which include that with periods of \sim 4.5–5.5 days at 55–100-m (centered at 85 m) depth, \sim 7.5–10 days at 50–100-m (centered at 80 m) depth, \sim 10–14 days at 0–80-m (centered at 40 m) depth, \sim 14–18.5 days above 50-m depth (surface intensified), \sim 17.5–23.5 days at 50–110-m (centered at 85 m) depth, and \sim 23.5–29 days

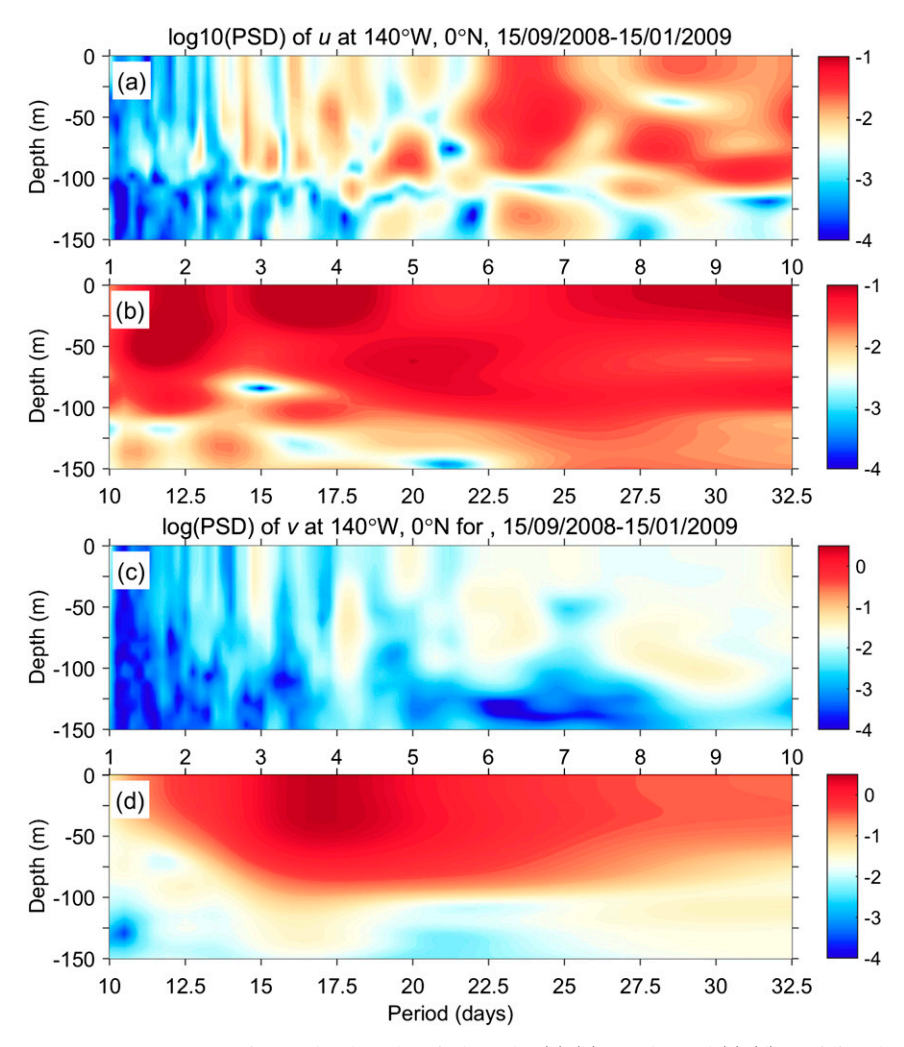


FIG. 1. PSD as a function of depth and periods of the (a),(b) zonal u and (c),(d) meridional v velocity components at 0° , 140° W, analyzed for the period of 15 Sep 2008–15 Jan 2009. Before calculation, u and v are normalized respectively by their absolute maximum during the time period analyzed (PSD unit is cpd $^{-1}$). Color bar ranges are [-4, -1] for (a) and (b) and [-4, 0.5] for (c) and (d).

above 50 m (surface intensified). Also, there were PSD peaks at periods between 1 and 4.5 days within 20–70-m depth (with multiple centers); not to be overdetailed, we collectively define them as one continuum. There were also PSD peaks at periods > 29 days; given the possible contribution from the 33-day, vortex mode TIW that was centered 4°–5° north of the equator (Lyman et al. 2007; Liu et al. 2019a), we loosely define the 29–45-day period band for part of that TIW. It means, nine waves (or wave continuums), manifested as zonal velocity oscillations, may coexist during this time period. (Within the certain period band of a wave, one or more extra PSD peaks at different depths might coexist; the peak either denotes a separate wave or suggests the successive antinode of the same wave.) In fact, the 14–18.5-day

wave has already been identified (Liu et al. 2019a; Lyman et al. 2007) and referred to as eTIW in literature (Liu et al. 2019a; note that the eTIW had a strong meridional counterpart in PSD, see Fig. 1d), and the 17.5–23.5-day wave at 50–100-m depth has also already known and referred to as subTIW (L19b).

In contrast, the meridional velocity (Figs. 1c,d) showed a lower variability below 10 days and a broad period band (10–30 days centered at \sim 14–19 days) with a surface-intensified vertical structure. Within the central periods, the amplitude was nearly uniform above 50-m depth, but dramatically vanishing toward the thermocline center (at \sim 100-m depth).

The nine waves seem to have well-separated period bands, with an exception between the surface-intensified

14–18.5-day wave and subsurface-intensified 17.5– 23.5-day wave, which overlapped in periods between 17.5 and 18.5 days. To isolate their individual effect, particularly of the surface- and subsurface-intensified structures, we determine the compromise borders in the period regime, and have isolated them from each other through bandpass filtering (with a Lanczos digital filter here; Duchon 1979). The filtering is made on the hourly velocity components, temperature, and buoyancy frequency squared (BFS, defined below), for the time period of 1 September 2008-31 January 2009. We have also conducted the 45-day low-pass filtering and the 1-day high-pass filtering to obtain the slowly varying background and high-frequency residual properties. The resulting nine individual waves, in terms of their oscillating velocities, during the same time period as the EQUIX experiment are shown in Figs. 2 and 3, and some of their statistical characteristics are summarized in Table 1. In addition, we make a reconstruction of the total velocity summing all the waves as well as the slowly varying background and high-frequency residual velocities (Fig. 4), which compares pretty well with the original velocities, indicating that the conducted filtering has not introduced significant velocity artifacts, and the identified wave components could explain most of the observed variance.

As evident in Figs. 2 and 3, these waves exhibited prominent features. First, during the EQUIX time period, some waves were manifested primarily as zonally oscillating velocities, while others were manifested primarily as meridionally oscillating velocities. For example, the wave W6 (i.e., the wave with a central period of 6.5 days; refer to Table 1 for the naming of the waves) had the maximum amplitude of $\sim 0.2 \,\mathrm{m\,s^{-1}}$ in u', larger than the maximum amplitude of v' ($\sim 0.1 \,\mathrm{m\,s}^{-1}$) by a factor of 2. Also, W12 had substantially larger maximum amplitude in u' ($\sim 0.12 \,\mathrm{m \, s}^{-1}$) than in v' ($\sim 0.05 \,\mathrm{m \, s}^{-1}$). The amplitudes in v' of both W17 (eTIW) and W20 (subTIW) were large, which were over ~ 0.6 and $\sim 0.3 \,\mathrm{m\,s^{-1}}$, respectively, while their maximum amplitudes in u' were only $\sim 0.1 \,\mathrm{m\,s^{-1}}$. The amplitude of W33 was also larger in v' ($\sim 0.2 \,\mathrm{m \, s^{-1}}$) than u' ($\sim 0.1 \,\mathrm{m \, s^{-1}}$). Among the others, W5, W9 and W25 had small amplitudes in both u' and v' ($\sim 0.05 \,\mathrm{m \, s^{-1}}$), while W3 had largest amplitude in both u' and v' (>~0.5 m s⁻¹), which might be due to strong transient waves. Second, the waves with the same period were not necessarily in phase between u' and v'. A typical wave was W17 (i.e., the eTIW), whose u' and v' were in phase above the thermocline (at \sim 100-m depth), forming the NE–SW oscillation viewed at a single location at the equator, and a NE-SW tilted horizontal circulation pattern associated with a Yanai wave from a bird's eye view (Liu et al. 2019a). The velocity components of W20 (i.e., the subTIW) were almost in phase, too. (The sum in v' of both W17 and W20 reaches $\sim 0.9 \,\mathrm{m\,s^{-1}}$, forming the observed energetic TIW.) By contrary, the velocity components of W6 seemed out of phase, but their maximum amplitudes seemed to be located at slightly different depths. Third, at some period bands, particularly at the short time periods (W3–W12), u' and v' might not coincide either in depth or in phase or in both, suggesting complex dynamics in terms of vertical and meridional modes of the equatorial waves (which is beyond the scope of the present work but discussed in the last section). Finally, we would like to note that, while most waves can be considered as a wave continuum, W3 actually was not, but consisted of multiple wave continuums with periods of 1–4.5 days, and different depths of peaks (Figs. 1a,b); the reason for combining them into one "wave" is for simplicity, because otherwise they are hardly separated.

A physically important feature was the variety of depths where the waves peaked, as already shown in the PSD distribution. W3, W5, W6, W9, and W20 clearly had subsurface amplitude peaks (varying from 50- to 85-m depths), while W6, W12, and W25 had two subsurface amplitude peaks (varying from 50- to 135-m depths). In addition, W9, W12, and W17 also had amplitude peaks at the surface. As will be shown below, above and below the subsurface amplitude maximum, the amplitude of the waves decreased (smoothly or abruptly) and resulted in out-of-phase velocity shears, which were crucial for the generation of complicated vertical structures of both the shear and mixing.

b. Decomposing the shear associated with identified equatorial waves

As mentioned above, both the eTIW and subTIW could induce large total shear squared changes (SSCs) due to coupling between the shear of the oscillating zonal velocity and the shear of the seasonal zonal flow (Liu et al. 2019a; L19b). Analogically, all the other equatorial waves could also induce significant SSCs due to their vertical shear in u'. In addition, the coexistence and hence the coupling among the equatorial waves, which were associated with significant velocity amplitudes at different depths, should further complicate the vertical structure of the shear above the thermocline. This will be investigated in detail in this subsection.

We now investigate the contribution of each identified wave to the total SS. For the zonal component, the total SS is calculated as $S_u^2 = (\partial u/\partial z)^2$, where u denotes the total zonal velocity which consists of a slowly varying background zonal flow \tilde{U} (defined as the 45-day low-pass filtered velocity in this study), the oscillating zonal velocities associated with the individual waves (denoted as u_3' , u_5' , ..., see below), and a high-frequency

residual flow u_R' (defined as the 1-day high-pass filtered velocity in this study). Similar treatment is done to the meridional component. (We note that it is appropriate to define the 45-day low-pass filtered velocity as the slowly varying background flow in the context of those rapidly varying waves; nevertheless, this background flow still contains variability at intraseasonal/seasonal to even longer time scales, and also exerts effects, which will be shown in section 3e.)

Following Liu et al. (2019a) and L19b, the contributions of the waves to the zonal SSCs relative to that of the slowly varying background flow can be expressed as

$$\Delta S_{u}^{\prime 2} = \underbrace{\left[\frac{\partial(\tilde{U} + u_{3}^{\prime} + u_{5}^{\prime} + \cdots)}{\partial z}\right]^{2}}_{S_{u}^{2}} - \underbrace{\left(\frac{\partial\tilde{U}}{\partial z}\right)^{2}}_{S_{\tilde{U}}^{2}}$$

$$= \underbrace{\left(\frac{\partial u_{3}^{\prime}}{\partial z}\right)^{2}}_{\Delta S_{u(3-3)}^{\prime 2}} + \underbrace{\left(\frac{\partial u_{5}^{\prime}}{\partial z}\right)^{2}}_{\Delta S_{u(5-5)}^{\prime 2}} + \underbrace{2\frac{\partial\tilde{U}}{\partial z}\frac{\partial u_{3}^{\prime}}{\partial z}}_{\Delta S_{u(\tilde{U}-3)}^{\prime 2}} + \underbrace{2\frac{\partial\tilde{U}}{\partial z}\frac{\partial u_{5}^{\prime}}{\partial z}}_{\Delta S_{u(\tilde{U}-5)}^{\prime 2}}$$

$$+ \underbrace{2\frac{\partial u_{3}^{\prime}}{\partial z}\frac{\partial u_{5}^{\prime}}{\partial z}}_{\Delta S_{u(3-5)}^{\prime 2}} + \cdots$$

$$(1)$$

Hereafter we will use expressions like $\Delta S_{u(\tilde{U}-3)}^{\prime 2}$ and $\Delta S_{u(\tilde{U}-3)}^{\prime 2}$, to denote the contribution from coupling between \tilde{U} and u_3^\prime , and between u_3^\prime and u_5^\prime , respectively; and so on (u_3^\prime) , for example, denotes the zonal velocity anomaly associated with W3; see Table 1 for the symbols). Also, we will use $\Delta S_{u3}^{\prime 2}$ to denote the contribution from solely the velocity anomaly, u_{3d}^\prime , i.e., $\Delta S_{u(3-3)}^{\prime 2} = (\partial u_3^\prime/\partial z)^2$; and so on. In addition, we use $S_{\tilde{U}}^2 = (\partial \tilde{U}/\partial z)^2$ to denote the SS of the slowly varying background zonal flow. The same is done to the meridional flow. With nine identified waves, one slowly varying background flow and one high-frequency residual flow, a total of 54 terms emerge according to rhs of (1) for either the u or the v component. A comparison of the magnitudes of these quantities enables us to identify the primary contributors to any specific aspect of the shear profile, in particular that in the WSL and UCL.

We first show the SS of the slowly varying background flow, the SS as a sum of all the zonal components (including the high-frequency residual flow, the slowly varying background flow and the flow associated with the individual waves), and the SSCs in both the zonal and meridional components due to all the waves in Fig. 5. The SS as a sum of all the zonal components (Fig. 5b) displayed almost the same pattern as the observed SS of the total zonal flow (Fig. 4 of I12).

Discrepancies were primarily located above 25-m depths, where velocity data were derived from extrapolations. Other small differences may result from the discrepancy between the TAO and EQUIX mooring locations, which would not affect the analysis here. Particularly, the observed suppressed shear at the WSL at ~50-m depth during 3–6 November and the observed enhanced shear in the UCL (75–100-m depth) during 1–6 November were well reconstructed by the combination of all the components.

The aforementioned SSCs in the WSL and UCL are evident in Fig. 5c, which demonstrates the primary contributions from the zonal velocity anomalies. For the WSL, the SS was indeed reduced around the ~50-m depth, but was also reduced within a wider range between 40- and 100-m depths. On the other hand, the UCL was not enhanced systemically between 70- and 100-m depths; rather, it was enhanced by u' in a 50-m-thick layer (~50–100-m depths) only during 2–3 November, and in a \sim 15-m-thick layer (90–105-m depths) on 4 and 6 November. The SSCs by v' (Fig. 5d) were relatively weak and generally positive in the upper thermocline, but were only significant in several 25-m thick patches in the UCL, including that between 95- and 110-m depths during 1–2 November, and ~85–105-m depths on 6 November. Obviously, u' or v' only induced transient enhancements in thin layers around \sim 100-m depth, which did not resemble the 50-m-thick, strongly sheared UCL as revealed in EQUIX. Instead, Fig. 5a suggests that the UCL was primarily maintained by the strong SS of the slowly varying background flow during this time period (1–7 November).

Other than the mentioned WSL and UCL, the large SS variations shown in other time periods and depths were also well reconstructed, such as the reduction during 24–25 October at 50–85-m depths, during 1–2 November at 50–80-m depths (which emerged as a strong WSL-like pattern), and the enhancement above the WSL (~25–40-m depths) during 3–7 November. During 7–8 November, the enhancement of SS between 40- and 80-m depths was reconstructed and was shown to include contributions from both the slowly varying background and the anomalous zonal velocities. Overall, it can be concluded that the vertical variations of the shear were primarily caused by the zonal, rather than meridional, wave-induced velocity oscillations.

c. Vertical and temporal structure of the shear: Formation mechanisms of the WSL and UCL

We focus now on the formation mechanisms of the WSL around ~50-m depths during 3–6 November and the UCL between 70- and 100-m depths during 1–6 November. We first examine the major contributors to the SSC averaged over a 10-m-thick and 1-day-long box typifying each of the WSL and the UCL. We plot the top 10 largest contributing terms, as well as the SS of the

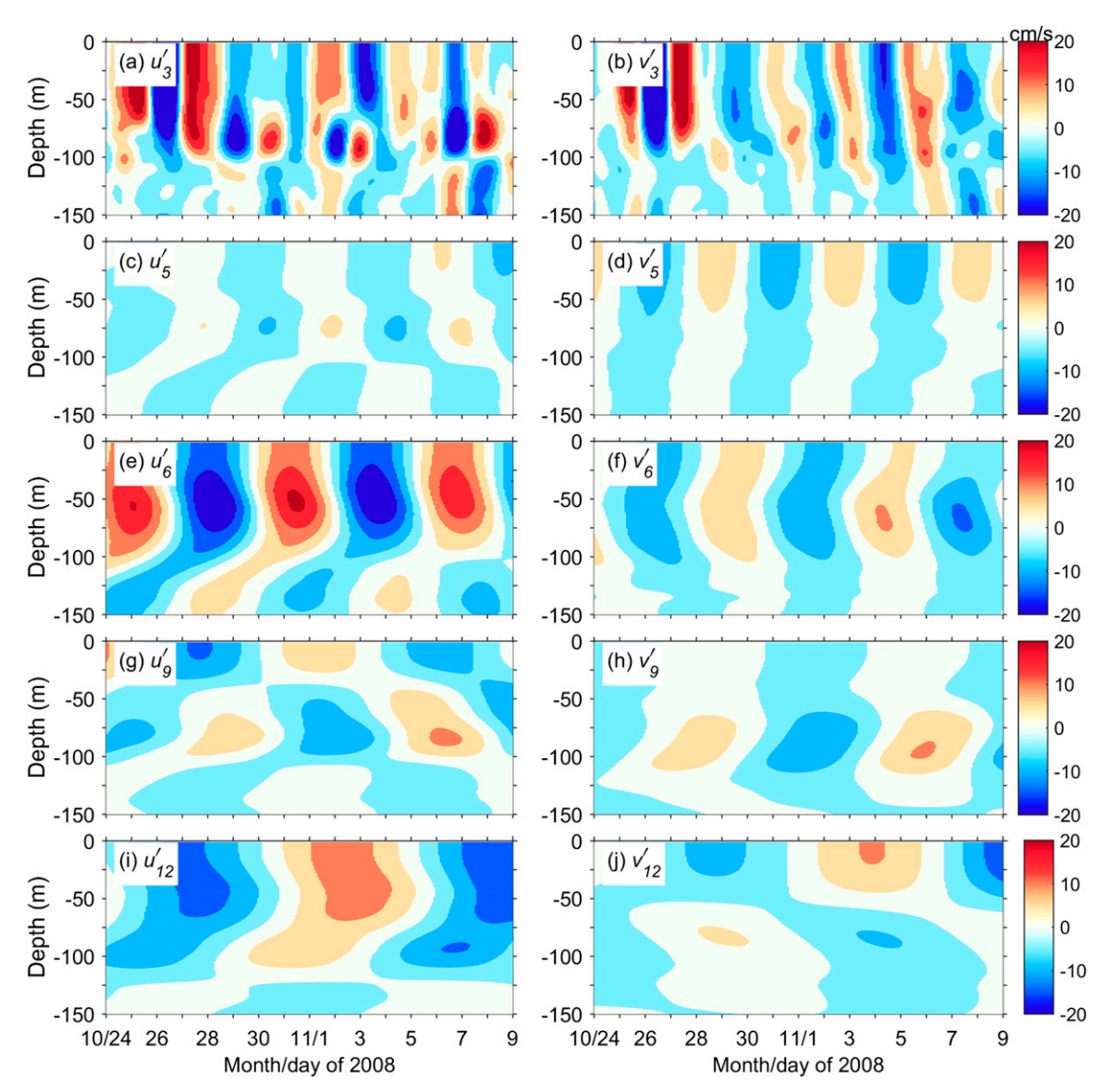


FIG. 2. The (left) zonal and (right) meridional oscillating velocities of the individual waves at 0°, 140°W, (the waves are denoted by panel title labels). The contour interval is 5 cm⁻¹. Each is bandpass filtered at its specific period band, which is listed in Table 1. The bandpass filtering is conducted at time period of 1 Sep 2008–31 Jan 2009, but only the results of the EQUIX time period (24 Oct–9 Nov 2008) are shown.

total and slowly varying background flow, in Fig. 6. The two boxes include that between 45- and 55-m depths during 0000–2400 UTC 4 November, and between 90- and 100-m depths during the same time period, and are referred to as Case WSL and Case UCL, respectively.

For the Case WSL (Figs. 6a,b), the final SS was \sim 1.49 \times $10^{-4} \, \mathrm{s}^{-2}$, while the SS of the slowly varying background flow was \sim 2.50 \times $10^{-4} \, \mathrm{s}^{-2}$. The reduction of the SS (\sim 1.0 \times $10^{-4} \, \mathrm{s}^{-2}$) was due to the coupling between the slowly varying background zonal flow \tilde{U} and the zonal velocity anomalies of several distinct waves, including W6, W5, W20, W12, W3, and W33 ($\Delta S_{u(\tilde{U}-6)}^{\prime 2} = -0.69 \times 10^{-4} \, \mathrm{s}^{-2}$, $\Delta S_{u(\tilde{U}-5)}^{\prime 2} =$

 $\begin{array}{l} -0.58\times 10^{-4}\,\mathrm{s}^{-2},\ \Delta S_{u(\bar{U}-20)}^{\prime2} = -0.55\times 10^{-4}\,\mathrm{s}^{-2},\ \Delta S_u^{\prime}\\ (\tilde{U}-12)^2 = -0.29\times 10^{-4}\,\mathrm{s}^{-2},\ \Delta S_{u(\bar{U}-3)}^{\prime2} = -0.24\times 10^{-4}\,\mathrm{s}^{-2}\\ \mathrm{and}\ \Delta S_{u(\bar{U}-33)}^{\prime2} = -0.13\times 10^{-4}\,\mathrm{s}^{-2},\ \mathrm{respectively});\ \mathrm{the\ coupling\ between\ }v_{17}^{\prime}\ \mathrm{and\ }v_{25}^{\prime}\ \mathrm{also\ contributed}\ \mathrm{(though\ was\ relatively\ small},\ \Delta S_{v(17-25)}^{\prime2} = -0.10\times 10^{-4}\,\mathrm{s}^{-2};\ \mathrm{in\ red\ in\ Fig.\ 6b}).\ \mathrm{The\ SS\ was\ enhanced\ by\ the\ interactions\ between\ }\tilde{U}\ \mathrm{and\ }u^{\prime}\ \mathrm{of\ two\ waves},\ \mathrm{W9\ and\ W17},\ \mathrm{and\ by\ solely\ }u_R^{\prime}\ (\Delta S_{u(\bar{U}-9)}^{\prime2}) = 0.47\times 10^{-4}\,\mathrm{s}^{-2},\ \Delta S_{u(\bar{U}-17)}^{\prime2} = 0.27\times 10^{-4}\,\mathrm{s}^{-2},\ \mathrm{and\ }\Delta S_{u(R-R)}^{\prime2} = 0.10\times 10^{-4}\,\mathrm{s}^{-2}).$ For the Case UCL (Figs.\ 6c,d), the final SS was\ en

For the Case UCL (Figs. 6c,d), the final SS was enhanced by $2.55 \times 10^{-4} \,\mathrm{s}^{-2}$ relative to the strong SS of the slowly varying background flow, from 3.96×10^{-4} to

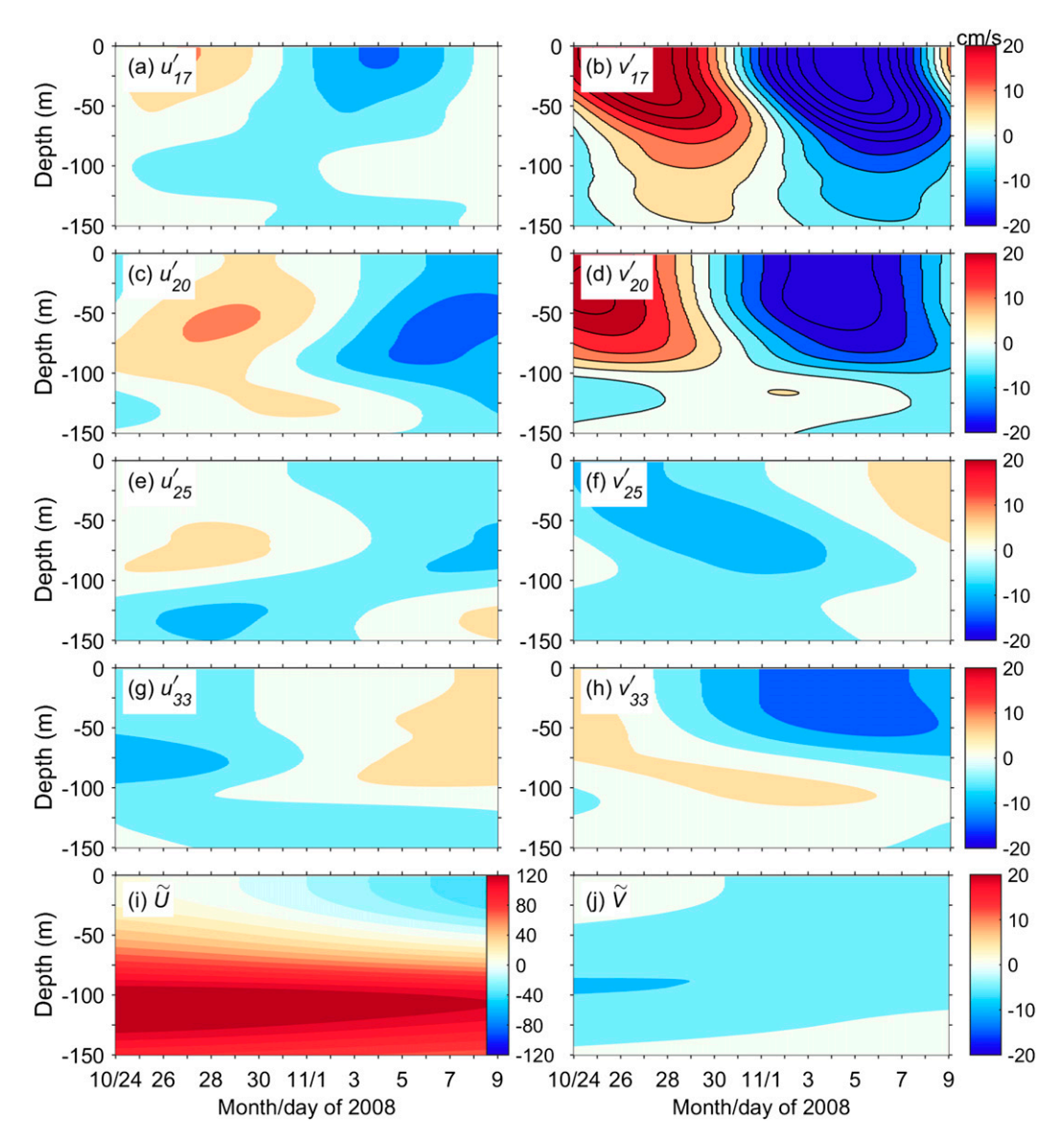


FIG. 3. (a)–(h) As in Fig. 2, but for the remainder waves. In (b) and (d), the values exceed the range in the color bar, so that contours are added (contour interval = 5 cm^{-1}). (i),(j) The slowly varying background (45-day low-pass filtered) zonal and meridional velocity components, respectively.

 $6.51 \times 10^{-4} \, {\rm s}^{-2}$. The sources were complex for this case. The increments resulted from the constructive interaction between the \tilde{U} and u' of W6, W20, W5, and W17 $(\Delta S'^2_{u(\bar{U}-6)} = 1.79 \times 10^{-4} \, {\rm s}^{-2}, \Delta S'^2_{u(\bar{U}-20)} = 1.11 \times 10^{-4} \, {\rm s}^{-2}, \Delta S'^2_{u(\bar{U}-5)} = 0.70 \times 10^{-4} \, {\rm s}^{-2}, \text{ and } \Delta S'^2_{u(\bar{U}-17)} = 0.39 \times 10^{-4} \, {\rm s}^{-2}),$ and from solely u'_R $(\Delta S'^2_{u(R-R)} = 0.51 \times 10^{-4} \, {\rm s}^{-2})$, as well as from solely v' of W20 $(\Delta S'^2_{u(20-20)} = 0.48 \times 10^{-4} \, {\rm s}^{-2})$; in red in Fig. 6d). These factors were opposed by the destructive interactions between \tilde{U} and u' of the W3, W33, and W12 $(\Delta S'^2_{u(\bar{U}-3)} = -1.04 \times 10^{-4} \, {\rm s}^{-2}, \Delta S'^2_{u(\bar{U}-33)} = -0.65 \times 10^{-4} \, {\rm s}^{-2}, \Delta S'^2_{u(\bar{U}-12)} = -0.63 \times 10^{-4} \, {\rm s}^{-2})$, and between v'_{20} and v'_3 $(\Delta S'^2_{v(3-20)} = -0.38 \times 10^{-4} \, {\rm s}^{-2})$.

The results demonstrate that, in both the WSL and UCL, most of the largest contributions (either positive or negative) were from the interactions between the slowly varying background zonal flow \tilde{U} and zonal oscillating velocities associated with the individual waves, indicating that not only the waves, but also the slowly varying background shear played a crucial role in inducing the total SSCs in the WSL. Nevertheless, in the UCL, W20 (the subTIW) also contributed to the enhanced SS via its own oscillating meridional velocities.

However, the joint contributions of the waves to SSCs vary periodically with time, leading to different combined results. In Fig. 7 we plot the time series of the

The number in the name indicates the central period of each equatorial wave

TABLE 1. Properties of the equatorial waves.

Equatorial waves ^a	Period band (days)	Depth range (m)	Symbols for u , v , T , and N^2 anomalies	$\operatorname{Max} u'$ amplitude (cm s ⁻¹)	Depths (m) of peak u' amplitude	$\operatorname{Max.} v'$ $\operatorname{Max} T'$ amplitude (cm s ⁻¹) amplitude (°C)	$\begin{array}{c} \operatorname{Max} T' \\ \operatorname{amplitude} (^{\circ} \mathrm{C}) \end{array}$	Depths of max T' amplitude (m)
W3	1–4.5	50-100	$u_3', v_3', T_3', N_3^{2'}$	27	85	49	0.5-1.5	75–110
W5	4.5–5.5	50–100	$u'_{\varsigma}, v'_{\varsigma}, T'_{\varsigma}, N^{2'}_{\varsigma}$	8 8	78	6	0.3	115
W6	5.5–7.5	20–70	$u_6', v_6', T_6', N_6^{2'}$	21	50	11	0.7	108
		110-150		7	130			
6M	7.5–10	50-100	$u_9', v_9', T_9', N_9^{2'}$	11	0	10	0.3	82
					80			
W12	10–14	0-80	$u_{12}',v_{12}',T_{12}',N_{12}^{2'}$	12	45	26	0.4	61
		80–115		10	93			
W17 (eTIW)	14–18	0-50	$u_{17}',v_{17}',T_{17}',N_{17}^{2'}$	11	0	61	0.8	91
W20	18-23.5	50 - 110	$u_{20}',v_{20}',T_{20}',N_{20}^{2'}$	13	85	28	0.4	76
(subTIW)								
W25	23.5–29	0-50	$u_{25}', v_{25}', T_{25}', N_{25}^{2'}$	2	0	8	0.2	75
		50 - 110		9	74		0.3	124
W33	29–45	0-50	$u_{33}',v_{33}',T_{33}',N_{33}^{2'}$	5	0	13	0.4	125
		50 - 110		8	78			

individual terms at both 50- and 95-m depths. At the 50-m depth, it was seen that during 7-8 November, most terms were on their positive phases (except for $\Delta S'^2_{u(\tilde{U}-20)}$, $\Delta S'^2_{u(\tilde{U}-12)}$, and $\Delta S'^2_{u(\tilde{U}-25)}$ which were weakly negative), resulting in greatly enhanced total SS; similar result emerged during 25-28 October. During 2–3 November, the positive $\Delta S'^2_{u(\bar{U}-3)}$, $\Delta S'^2_{u(\bar{U}-5)}$, and $\Delta S'^2_{u(\bar{U}-6)}$ were larger in magnitude than the negative $\Delta S'^2_{u(\bar{U}-20)}$, $\Delta S'^2_{u(\bar{U}-12)}$, and $\Delta S'^2_{u(\bar{U}-9)}$, leading to enhanced SS. During 30 October-1 November, by contrast, four terms with larger magnitudes were on their negative phases and the other four terms with smaller magnitudes on their positive phases, leading to weakly reduced total SS. Similarly, at the 95-m depth, the enhanced SS during 28–29 October, 1–2 November, 6– 7 November, and reduced SS during 27-28 October, 30-31 October, and 7-8 November, could be well explained via the combination of specific waves.

The vertical variations of the waves and differences of their vertical scales also led to the complexity of the combined results in SSCs. To illustrate this, we plot the shear of the oscillating zonal velocities, i.e., $\partial u_3'/\partial z$, ..., and the corresponding SSCs due to its interaction with \tilde{U} , i.e., $\Delta S_{u(\tilde{U}-3)}^{\prime 2} = 2\partial \tilde{U}/\partial z(\partial u_3^{\prime}/\partial z), \ldots$, in Figs. 8 and 9. Several basic features can be inferred from the figures. One is that the sign of the SSCs was always opposite to (the same as) the sign of the shear of the waves above (below) the EUC core, due to multiplication by the negative (positive) shear of the slowly varying background flow, $\partial U/\partial z$, indicating again the importance of the shear direction of the oscillating zonal velocity of each wave. The second was that, ~20-30 m above the EUC core, the amplitude of the SSCs was enhanced for all waves due to the strong shear of the slowly varying background flow, providing the potential for the waves to enhance or reduce the total SS at these depths. On the other hand, vertical pattern of the SSCs varied from wave to wave. First, either above or below the EUC core, a two-layer structure with nearly antiphase SSCs could occur, with the transition depth the same as that of the maximum amplitude of u', particularly for the subsurface-intensified waves, such as W5, W6, W12, W20, and W25; however, this feature was ambiguous if a surface-intensified wave or another subsurface-intensified wave coexisted at the same period band, such as W3, W9, and W17. Second, the vertical scales of not only the twolayer structure, but also each layer, varied from wave to wave, too, ranging between 50 and 70 m, and between 20 and 55 m, respectively. All these features led to the complexity of the total combined pattern of the SS changes. Table 2 summarizes these characteristics.

Overall, the differences in periods, in depths, and in vertical scales of the waves, together with the slowly

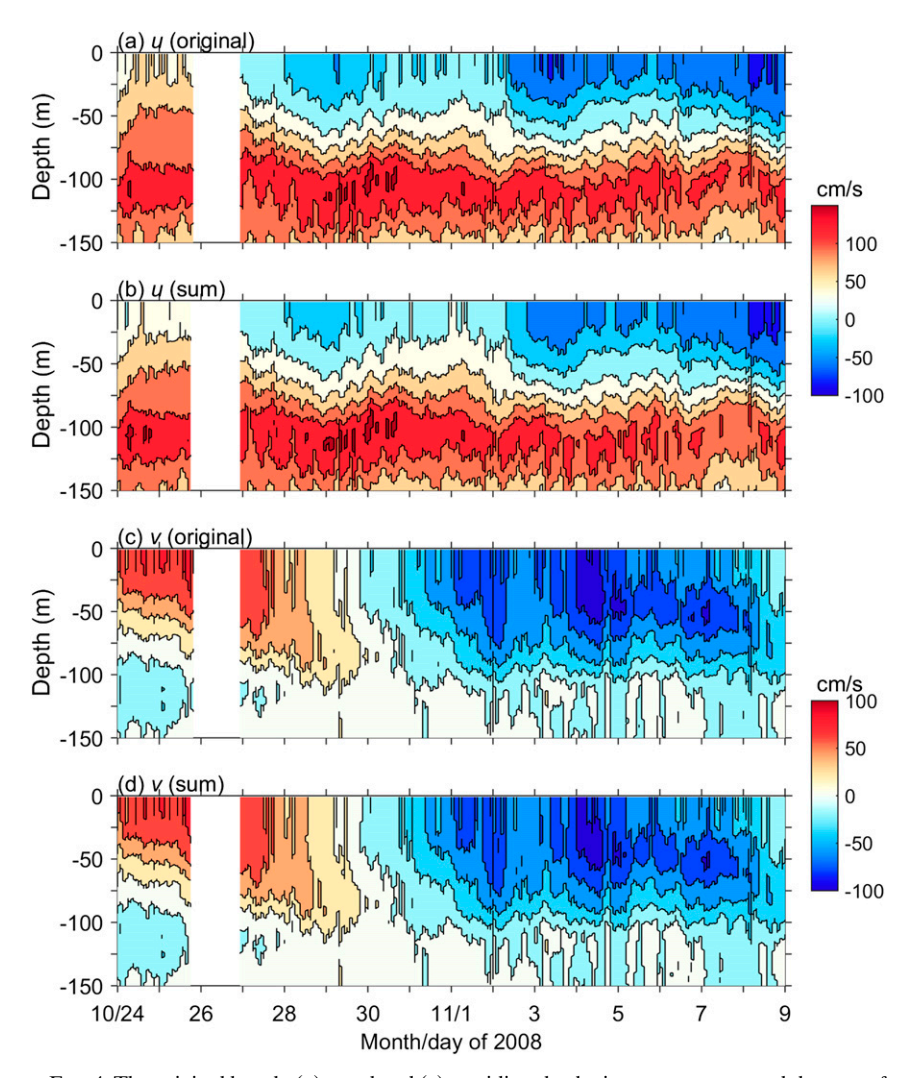


FIG. 4. The original hourly (a) zonal and (c) meridional velocity components, and the sum of the bandpass filtered, slowly varying background and high-frequency residual (b) zonal and (d) meridional components, for the EQUIX time period at 0°, 140°W.

varying background flow, lead to a variety of combined vertical structures of the shear; among them the EQUIX-observed WSL and UCL structure could only be a specific one, which stood out due primarily to the joint contribution from W3, W5, W6, W12, and W20. Particularly, the subsurface-intensified waves, i.e., W5, W6, and W20, contributed largely to the formation of both layers.

d. Shear instability in the WSL and UCL: Modulation of the associated ΔN^{2}

In the present section, we extend the analysis to the reduced shear squared changes (RSSC) associated with the waves. We only focus on zonal components of the waves because they were dominant as shown above. The zonal RSSC $\Delta S'^2_{\text{ured}}$ is defined as $\Delta S'^2_{\text{ured}} = \Delta S'^2_u - 4N^2$. This property represents the tendency of the waves to induce shear

instability (and thus turbulence and mixing) due to not only the associated velocity shear, but also the associated density strain (Holmes and Thomas 2015). When $\Delta S'^2_{\rm ured} > (<)0$, the wave tends to destabilize (stabilize) the flow. Here, N^2 is the anomalous BFS bandpass filtered at the specific period bands of the waves (denoted as $N_3^{2'}$, $N_5^{2'}$, ..., hereafter; also see Table 1 for the symbols; note that, unlike $\Delta S'^2_u$, no coupling between waves or between wave and mean flow took place in forming $N^{2'}$, because $N^{2'} \sim \partial T'/\partial z$). In the meanwhile, the RSS of the slowly varying background zonal flow is defined as $S^2_{\tilde{U}{\rm red}} = S^2_{\tilde{U}} - 4\widetilde{N^2}$, where $S^2_{\tilde{U}}$ is the SS associated with the slowly varying background zonal flow \tilde{U} , and the $\widetilde{N^2}$ is the BFS associated with the slowly varying background density.

We first show $\Delta S_{\text{ured}}^{\prime 2}$ during the EQUIX time period along with the RSS of the slowly varying background

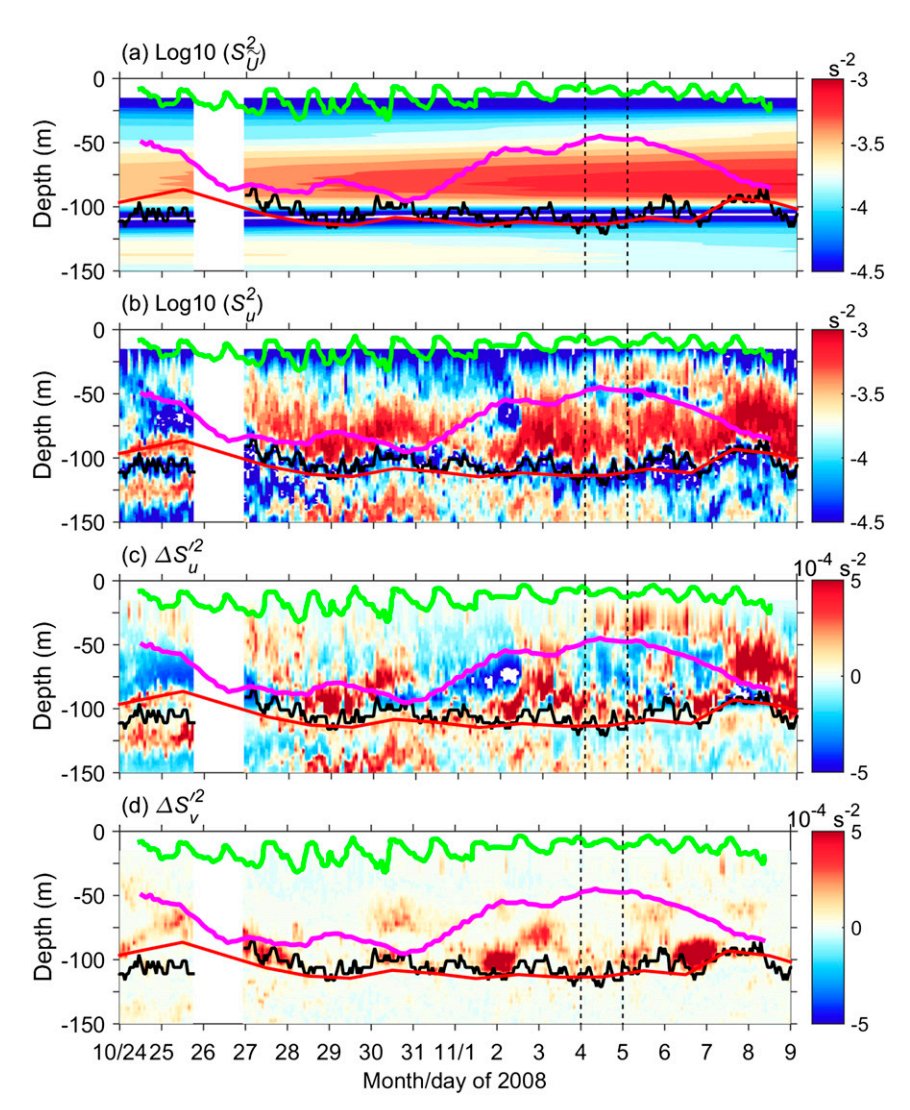


FIG. 5. Shear squared and anomalies for the EQUIX time period at 0°, 140°W. Shear squared of (a) the slowly varying background zonal flow, (b) total shear squared calculated as the sum of all 54 terms of the zonal velocity (see text), (c) total shear squared calculated as the sum of all terms of the zonal velocity except for that of the slowly varying background zonal flow, i.e., the difference between (b) and (a), and (d) as in (c), but for the meridional velocity. The thick green and pink lines denote the bases of the ML and DCL, respectively, adapted from I12; the black and red lines denote the daily depths of the EUC core and 20°C isotherm, respectively; the two dashed vertical lines denote the time period of 4 Nov 2008.

zonal flow, $S^2_{\bar{U}{\rm red}}$, as well as the total changes on the SS and BFS in Fig. 10. In the layer above ~85-m depth, the $S^2_{\bar{U}{\rm red}}$ was around 0 (Fig. 10a), confirming that this layer was marginally stable (Smyth and Moum 2013) and could become unstable subject to small changes in $\Delta S^{\prime 2}_u$ and/or $N^{2'}$. The $S^2_{\bar{U}{\rm red}}$ between 100- and 150-m depths, in contrast, was strongly negative (Fig. 10a), indicating that this layer was generally stable, and could turn unstable only in conditions of great enhancement (reduction) of $\Delta S^{\prime 2}_u$ ($N^{2'}$).

The $\Delta S_{\text{ured}}^{\prime 2}$ pattern, particularly with large magnitudes, generally resembled that of the $\Delta S_u^{\prime 2}$ (Figs. 10b,d,

respectively), meaning that the former was primarily determined by the SSCs. For example, $\Delta S_{\rm ured}^{\prime 2}$ was mostly positive in the deep depths of the UCL during 1–4 November, income 50–100-m depths during 28–30 October and 7–9 November, above the WSL (20–40-m depths) during 4–6 November, and was continuously positive at \sim 50–100-m depths during 2–3 November. In addition, $\Delta S_{\rm ured}^{\prime 2}$ was positive below 100 m during 24–25 October and 28–31 October. Those were all similar to the signs of ΔS_u^2 .

Above the thermocline center, the aforementioned depths and times of enhanced shear were in good

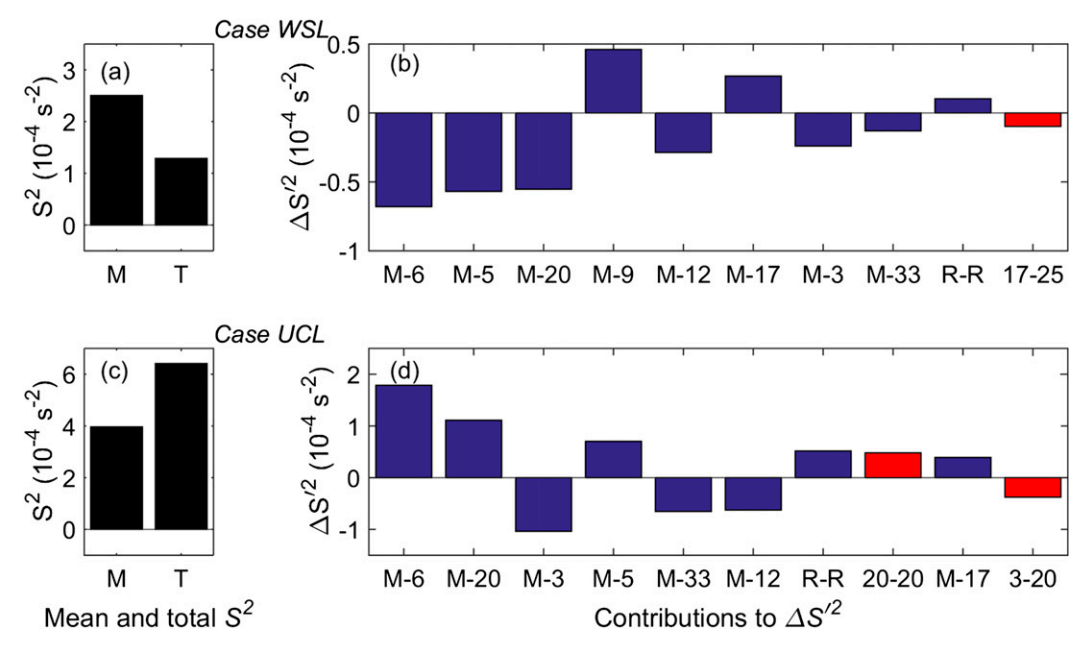


FIG. 6. (left) Depth and time averaged shear squared of the slowly varying background (M) and total (T) flow, and (right) 10 largest contributions to the shear square changes from some individual waves, averaged over (top) 45–55-m depths during 0000–2400 UTC 4 Nov, and (bottom) 90–100-m depths during 0000–2400 UTC 4 Nov. Blue (red) bars denote contributions from the zonal (meridional) velocity components. Here, "M-3" denotes the contribution of W3 via interaction with the slowly varying background flow, i.e., $2(\partial \tilde{U}/\partial z)\partial u_3'/\partial z$, which is denoted as $\Delta S_{u(\tilde{U}-3)}^{(2)}$ in the text, and so on; "R-R" denotes the pure contribution from the high-frequency residual flow, i.e., $\Delta S_{u(R-R)}^{(2)} = (\partial u_R'/\partial z)^2$, and so on.

agreement with those of strong mixing shown by the EQUIX experiment. Those below the thermocline were also associated with more mixing than other time periods as shown by the EQUIX experiment. These results demonstrate that the positive $\Delta S'_{\rm ured}^2$ indeed destabilized the flow and led to enhanced mixing. By contrast, the $\Delta S'_{\rm ured}^2$ was negative and had large magnitude in 50–80-m depths, during 24–25 October, in the layers just above the EUC core during 27–28 October, 30–31 October, and 7–8 November; particularly, it was negative and had moderate magnitude in the WSL during 4–7 November. Those layers were associated with greatly reduced or even completely suppressed mixing, which is also in good agreement with the EQUIX measurements.

Nevertheless, $N^{2'}$ also modulated the zonal RSS pattern and contributed to mixing in the WSL and UCL (Fig. 10c). In the upper 50-m depths (embracing the WSL) of 4–6 November, $-4N^{2'}$ was negative, enhanced the negative RSSC in the WSL but did not reverse the sign above it; in the UCL (75–100-m depths of 3–6 November), on the other hand, $-4N^{2'}$ was positive and enhanced the positive RSSC. Also, in the thin layer at \sim 100-m depth of 1–2 November, $-4N^{2'}$ reinforced $\Delta S_u^{\prime 2}$ and led to larger positive RSSC; in the 25–75-m depths of 28–31 October, the weak positive $-4N^{2'}$ slightly enhanced the weak SSCs therein, leading to sign reversion occasionally. However,

note that during most of the EQUIX time period (27 October–6 November), the magnitude of $-4N^{2'}$ in the upper thermocline was several factors smaller than that of $\Delta S_u^{\prime 2}$, thus only played a modulating, but not controlling role, in constituting the RSSCs. In contrast, between 50-and 150-m depths on 24–25 October, and below 110- and above 50-m depths on 7–8 November, $\Delta S_{\text{ured}}^{\prime 2}$ was governed by $N^{2'}$ to a larger extent (Figs. 10b–d).

To gain a further understanding of $N^{2'}$ associated with each individual wave, and to explain their contributions to $\Delta S'^{2}_{\text{ured}}$ at specific depths and time periods, we also calculate the bandpass filtered temperature T' at the specific period bands of the waves (denoted as T'_3, T'_5, \ldots , hereafter; also see Table 1 for the naming of the symbols). The variations of T' are shown in Figs. 11 and 12 along with the corresponding $N^{2'}$. Two basic features are evident: one lies in phase differences between the shear (or u' and v') and strain (or T'), and the other lies in the vertical patterns of the strain (or T').

First, among the detected waves, two classes can be identified in terms of phase differences. One is typified by W17 (i.e., the eTIW) and W20 (i.e., the subTIW), which had larger amplitude in v' than u' (Fig. 3), and a phase lag of $\pi/2$ of T' (and $N^{2'}$) to v' (Figs. 12a,b). This feature indicates that they could be resulted from a southward-shifted Yanai wave. The $\pi/2$ phase-lag relation between $N^{2'}$ and v'

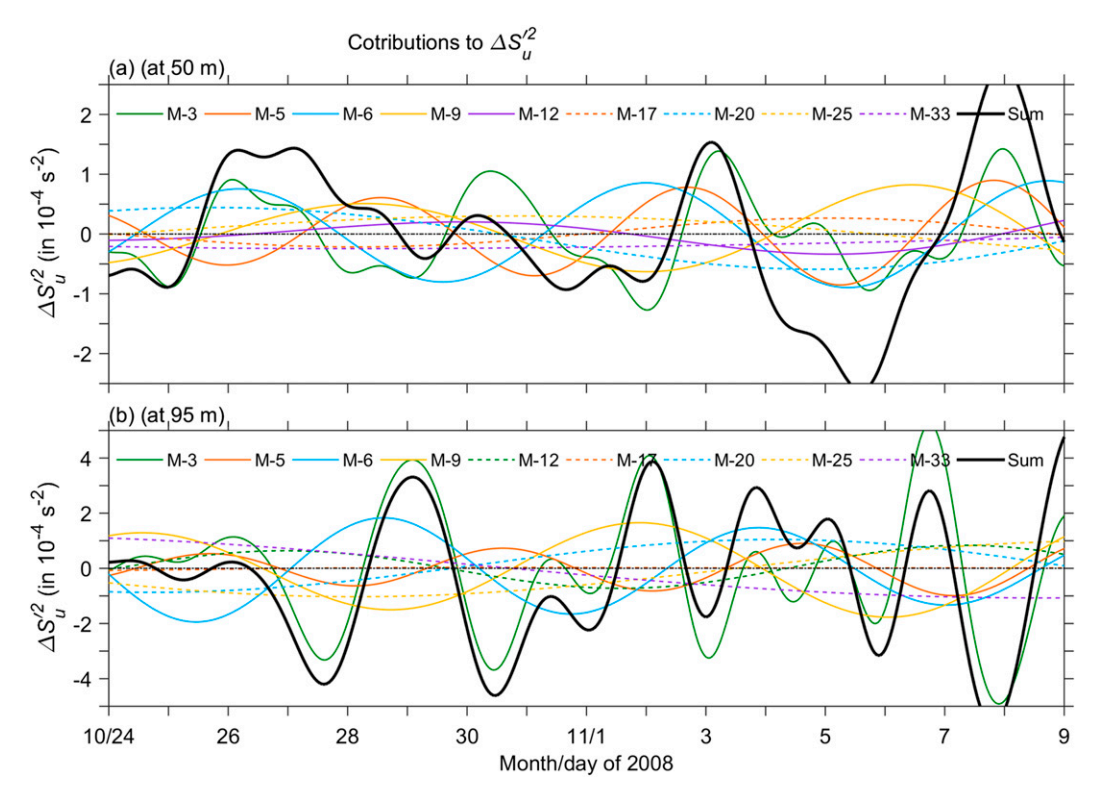


FIG. 7. Contributions to the shear squared changes from the coupling between the slowly varying background zonal flow and the individual waves, and their sum (denoted in insets, refer to caption of Fig. 6 for details) at a WSL depth (50 m) and a UCL depth (95 m), for the EQUIX time period at 0°, 140°W.

seemed also to exist at W25 and W33 (Fig. 12). The second class, represented by W6, showed larger amplitude in u' than v' (Fig. 2), and out-of-phase variation (phase lag by π) between T' and u' (Figs. 11e,f). This kind of relation was also evident in W9 (only below 50 m) and W12 (Fig. 11).

The second feature was that, like the SSCs, the $N^{2'}$ also showed varying vertical patterns and scales. In the surface-intensified W17 (the eTIW) and the subsurface-intensified W20 (i.e., the subTIW), T' and $N^{2'}$ varied on large vertical scales relative to other wave types. The peak of their T' was located at the thermocline center (at ~100-m depth), and extended upward and downward, leading to a two-layer structure of $N^{2'}$, with opposite signs between the two layers and the thermocline center as their border. Specifically, the T' of W17 extended upward to the surface and downward to about 140-m depth, resulting a 75-m-thick $N^{2'}$ layer both above and below the thermocline center, with two peaks in $N^{2'}$ at ~50- and \sim 125-m depth. The T' of W20 extended upward to ~50-m depth and downward to ~150-m depth, resulting in a 50-m-thick $N^{2'}$ layer both above and below the thermocline center, with peaks in $N^{2'}$ at \sim 50–80-m depth and \sim 110–125-m depth. On the other hand, the higher frequency waves shown in Fig. 11, such as W6, W9, and W12, had smaller scale T' and $N^{2'}$. The peak and vertical extents of T' nearly coincided with those of u' (out of phase; Figs. 2, 11), leading to a two-layer structure of $N^{2'}$ with opposite signs between the two layers, but with small vertical extents for each layer and varying border depths (ranging between 65- and 85-m depths). This led to simultaneously opposite signs of $N^{2'}$ in the upper thermocline. (The features in u', v', and T' indicate that these waves may belong to either gravity or Rossby or combined (i.e., Yanai) type of equatorial waves, considering possible slight meridional shift of them, yet to be verified).

Returning to the representative WSL and UCL depths (50 and 95 m, respectively; Fig. 13), we find that during 4–6 November at 50-m depth, most of the waves, including W3, W9, W20, W25, and W33 induced negative (stabilizing) $-4N^{2'}$, while W6 and W17 induced positive (destabilizing) $-4N^{2'}$. In total, they led to negative $-4N^{2'}$ during the short period and contributed to the reduction of RSSCs at the WSL (Figs. 13a,c). During 1–6 November, the total $-4N^{2'}$ was generally positive, contributing to the enhanced instability of the UCL (Figs. 13b,d). Positive $-4N^{2'}$ was primarily due to three waves: W12, W20, and W25, while W33 induced negative $-4N^{2'}$, and both W3 and W5 changed sign during that time period. However, the magnitude of $-4N^{2'}$ was

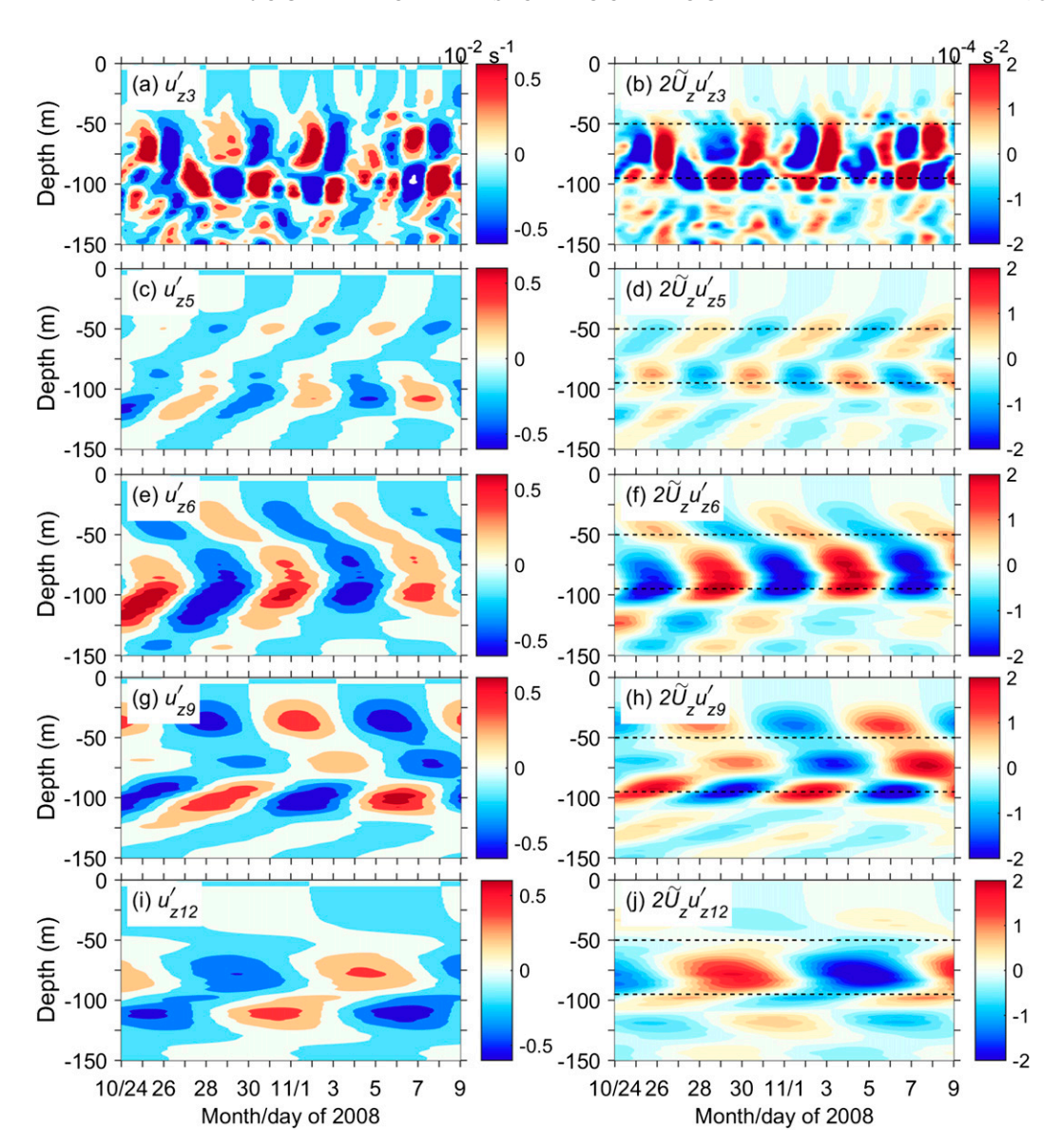


FIG. 8. (left) Shear of the zonal velocity associated with each individual wave. (right) Shear squared changes from the interaction between the slowly varying background zonal flow and the waves. Here, $2\tilde{U}_z'u_{z3}' = 2(\partial \tilde{U}/\partial z)\partial u_3'/\partial z$, and is denoted also as $\Delta S_{u(\tilde{U}-3)}^{\prime 2}$ in the text; and so on. The individual waves are denoted in insets. The two dashed lines denote 50- and 95-m depths. Shown are for the EQUIX time period at 0° , 140° W.

generally smaller than $\Delta S_u^{\prime 2}$ (comparing with Fig. 7) in the upper thermocline, so that the stratification anomalies did not crucially influence $\Delta S_{\text{ured}}^{\prime 2}$.

e. Slowly varying background shear in the UCL: Modulation from a longer-time-scale equatorial wave

Figure 5b showed that the total SS was enhanced around the UCL depths and time period, 2–9 November; however, the SSCs induced by the aforementioned waves were negative in a large portion of the UCL during 3–7 November (except for some layers just above the EUC

core), and thus did not contribute to this systematic enhancement. The systematic enhancement instead existed in the background flow (Fig. 5a). A question therefore arises as to what caused the SS enhancement during the late half of the EQUIX experiment. The answer turns out to be an (irregular) wave-like process with a period of 50–90 days (or a combination of waves with ~ 50 -day period in the mixed layer and ~ 90 -day period in the thermocline) manifested also in zonal velocity oscillation at the central EUC depths (Figs. 14a,b; the meridional velocity only displayed a weak ~ 50 -day oscillation in the

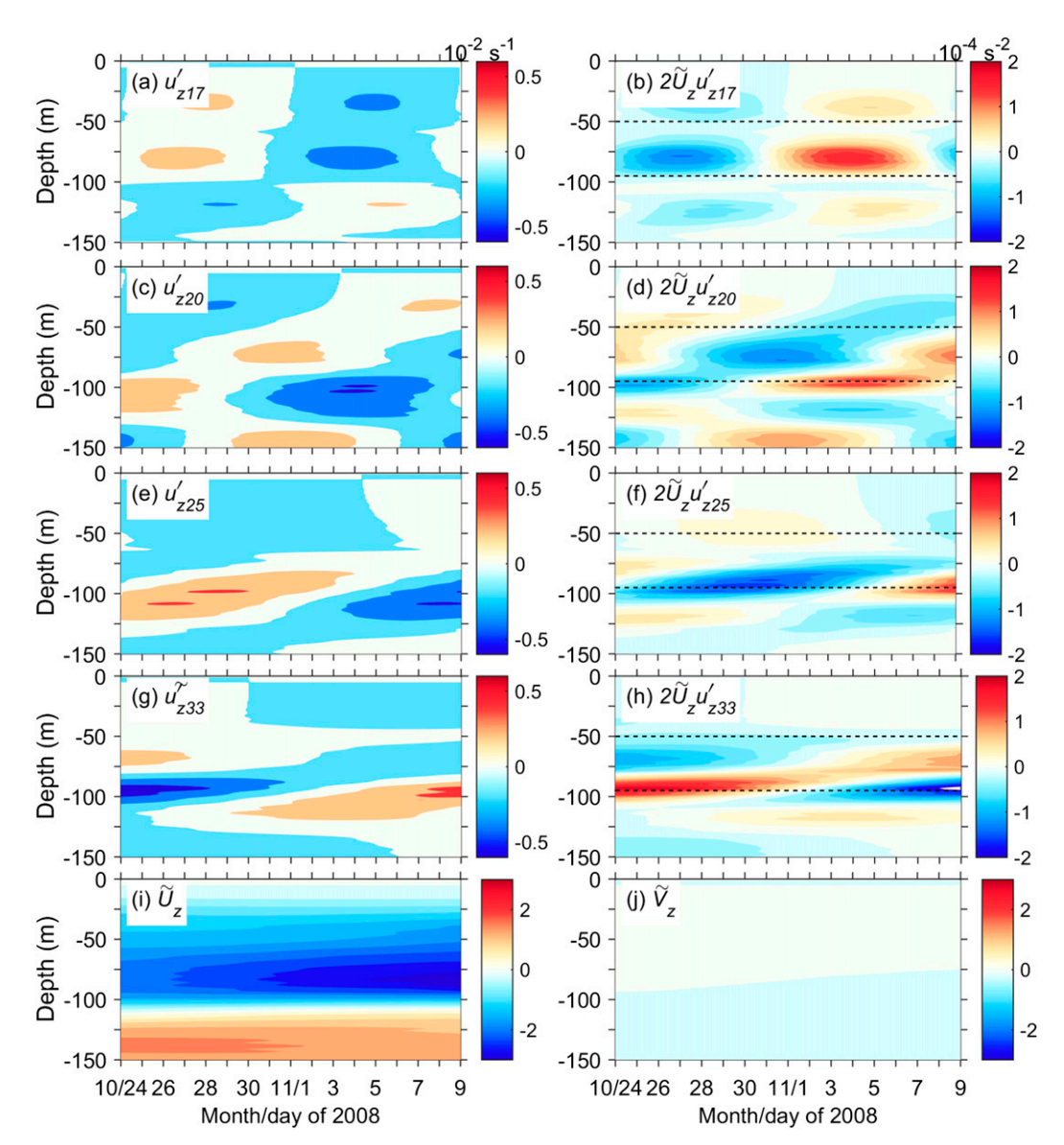


FIG. 9. (a)–(h) As in Fig. 8, but for the remainder waves, (i)–(j) The shears for the slowly varying background zonal and meridional flow, i.e., $\tilde{U}_z = \partial \tilde{U}/\partial z$ and $\tilde{V}_z = \partial \tilde{V}/\partial z$, respectively.

mixed layer). Indeed, it is seen from 50- to 90-day bandpassed and $3.5^{\circ} \times 3.5^{\circ}$ smoothed (Delcroix et al. 1991) sea level anomaly data that a Kelvin wave passed by during the measurements (not shown). Its period is so long that it is not detected from the PSD analysis conducted here (Fig. 1), and was therefore taken as part of the slowly varying background flow. The process led to a variation of $\Delta S_u^{\prime 2}$ with amplitude of about $5 \times 10^{-4} \, \text{s}^{-2}$ within 50- and 100-m depths. It was increased from its moderate value to its maximum during the EQUIX time period, with an increment of SSC of about $3 \times 10^{-4} \, \text{s}^{-2}$, controlling the coherent enhancement of the SS in the entire UCL.

Similar to other waves, this wave-like process was also associated with changes in T and N^2 (Figs. 14c,d). The temperature in the thermocline seemed to be highest (the isotherms lowered most) at the eastward-to-westward transition phase of u' (note that u' here denotes the anomalous zonal velocity of this process), decreased during the entire phase of westward u', and got minimal (the isotherms elevated most) at the westward-to-eastward transition phase of u'; it was increased during the entire phase of eastward u'. In another word, there was a phase lag of π between u' and T'. Moreover, N^2 was largest during the phase of the isotherm stretches. However,

TABLE 2. Statistics of changes in the shear squared and buoyancy frequency squared induced by the equatorial waves and their vertical	1
scales	

Equatorial waves	Max amplitude of $\Delta S'^2_{u(\tilde{U}-x)} \big[= 2 (\partial \tilde{U}/\partial z) \partial u'_x/\partial z \big] $ $ (10^{-4} \mathrm{s}^{-2})$	h_1 : depth (m) of the peak amplitude of $\Delta S'^2_{u(\tilde{U}-x)}$	h_2 : depth (m) of the secondary (third) peak of $\Delta S'^2_{u(\tilde{U}-x)}$	Distance between h_1 and h_2 (m)	Max amplitude of $4N^{2'}$ (10^{-4}s^{-2})	h ₃ : depth (m) of the peak amplitude of 4N ²	h_4 : depth (m) of the secondary (third) peak of $4N^{2'}$	Distance between h_3 and h_4 (m)
W3	10.1	71	95	24	1.6-3.2	125	75 (59)	50 (66)
W5	1.1	90	50	40	0.7	81	33 (126)	48 (45)
W6	4.6	93	48	45	0.8	62	104	42
W9	3.5	96	75 (39)	21 (57)	0.9	103	60	43
W12	3.8	79	99 (37)	20 (42)	0.8	92	40	52
W17 (eTIW)	1.6	79	37	42	2.0	125	55	70
W20 (subTIW)	1.2	96	74 (42)	22 (54)	1.0	80	125	45
W25	1.5	94	47 (122)	47 (28)	1.2	100	55	45
W33	1.9	94	71	23	0.7	88	50	38

during the EQUIX time period, the temporal variation of N^2 was below 0.3×10^{-4} s⁻², only providing small modulation of the RSSC.

f. Relationship of the WSLs and UCLs to TIW phases

Since the UCL-WSL structure was only observed once, and happened to emerge during the N-S transition phase and the S phase of the specific TIW (I12), it might be simply supposed that this two-layer structure could only occur in those two phases. The analyses in the above sections indicate that the formation of the UCL-WSL structure (or either one of them) is subject to an appropriate combination of certain equatorial waves, in terms not only of their depths of maximum zonal velocity anomaly, vertical scales and phases (in inducing appropriate shear), but also of the wave types (in inducing appropriate density strain). Clearly, the normally recognized, surface-intensified eTIW alone would not be able to induce such a complicated vertical structure, although it may contribute. In this subsection, we extend the study time period to 1 October-31 December 2008 to identify more occurrences of the WSL-UCL structure and draw more general conclusions about its origin.

We show the 45-day high-pass filtered properties, including u', v', $\partial u'/\partial z$, $\Delta S_u^{\prime 2}$, $-4N^{2\prime}$, and $\Delta S_{\text{ured}}^{\prime 2}$, in Fig. 15. Those anomalies include most of the possible waves. The normally recognized TIWs could be loosely represented by the surface-intensified meridional velocity oscillations, v' (Fig. 15b); in addition, v' had a loose coincidence with u' (i.e., u' and v' in phase; Fig. 15a). Note also the temporal and vertical variations of u', which indicated the multiple-time-scale equatorial waves with different depths of u' peaks. As demonstrated in the

above sections, ΔS_u^2 had opposite sign to $\partial u'/\partial z$ above the EUC core, and its amplitude was enhanced 20–30 m above it (Figs. 15c,d). As with the individual wave motions, variations in $\Delta S_{\text{ured}}^{\prime 2}$ were mostly caused by velocity shear rather than density strain.

We detected 10 more WSL-UCL structures, defined as not only negative in ΔS_u^2 , but also negative in ΔS_{ured}^2 in the WSL and positive $\Delta S'_{ured}$ in the UCL (note that owing to the marginally stable nature of the mean flow, Fig. 10a, $\Delta S_{\mathrm{ured}}^{\prime 2}$ can approximate the total RSS and its positive/negative sign can indicate instability/stability of the flow). The overall potential 11 WSL structures, some of which were shallow and the others were deep, were shown by black boxes in Figs. 15b, 15d, and 15f. It is clear that they occurred not only during N-S and S phases of the TIW, but also during northward (N) and southward-to-northward (S-N) phases, as shown in Fig. 15b. The results demonstrate that the WSL-UCL structure, or either of them, can emerge due to the couplings of the waves. However, the periods of the equatorial waves vary from days to nearly a month, making the duration of the coincidently resulted WSL or UCL usually short.

4. Summary and discussions

We have studied the formation mechanisms of a weakly sheared, essentially nonturbulent, \sim 10-m-thick layer at \sim 50-m depth, and a strongly sheared, turbulent, \sim 30-m-thick layer just above the EUC core (at \sim 75–105 m), observed in part of EQUIX (24 October–9 November 2008; M09) at 0°, 140°W in the eastern equatorial Pacific. The layers persisted only for several days (on 4–7 November and

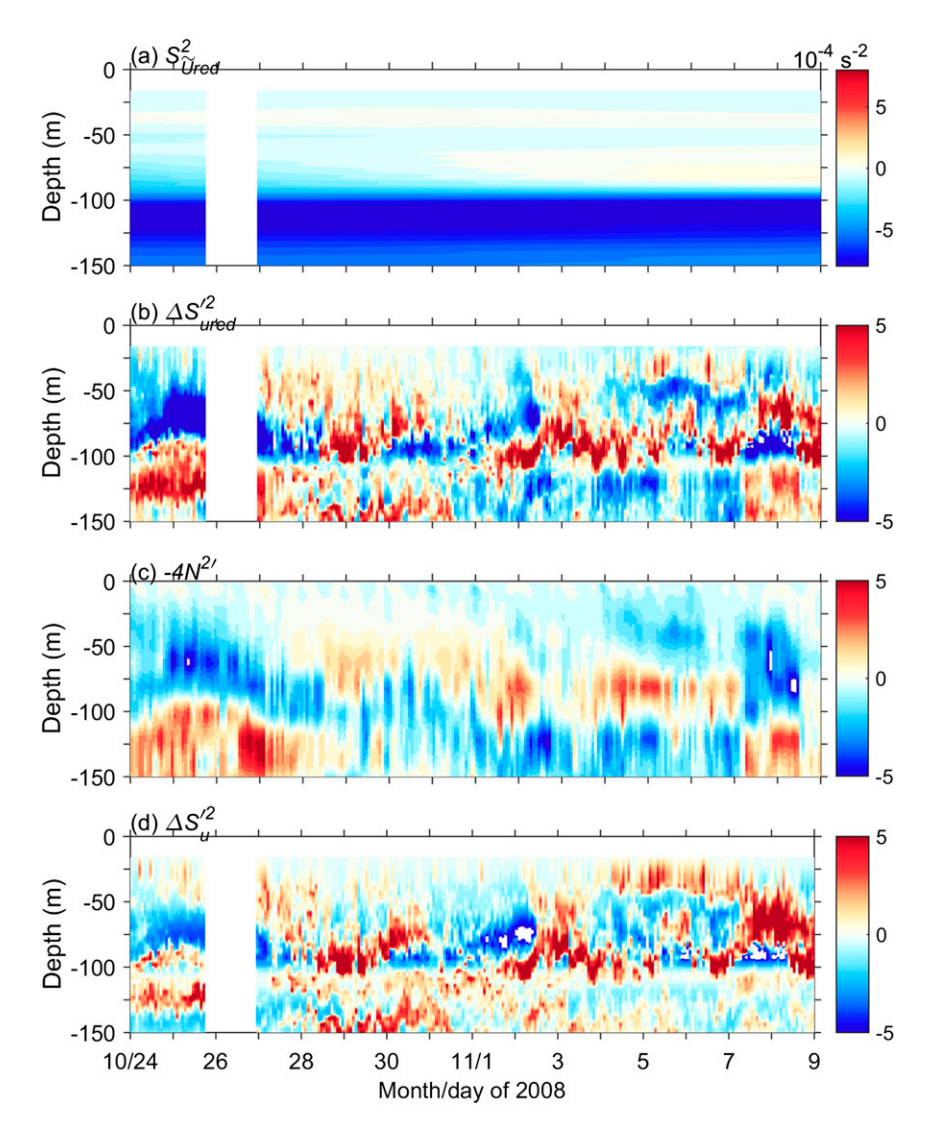


FIG. 10. Reduced shear squared and its contributions. (a) Reduced shear squared from the slowly varying background shear squared and buoyancy frequency squared, calculated as $\Delta S_{\tilde{U}\text{red}}^2 = \Delta S_{\tilde{U}}^2 - 4\tilde{N}^2$. (b) Changes of reduced shear squared contributed from both the shear squared changes and buoyancy frequency squared changes, calculated as $\Delta S_{\text{ured}}^{\prime\prime} = \Delta S_u^{\prime\prime} - 4N^{\prime\prime}$. (c) Buoyancy frequency squared changes (×-4), and (d) shear squared changes of all the oscillating zonal velocities $\Delta S_u^{\prime\prime}$, which is the same as Fig. 5c, but shown here for comparison purpose: (b) = (c) + (d). Shown are for the EQUIX time period at 0°, 140°W.

1–6 November, respectively). These were referred to as the weak shear layer (WSL) and the upper core layer (UCL), respectively. We focused on the mechanisms of shear reduction/enhancement in the layers, and of suppression/emergence of the instability and thus mixing therein. The hourly velocity and temperature data at the same site collected by the TAO mooring array are employed for the analysis. The main results are summarized as follows.

First, we identified equatorial waves on multiple time scales during the EQUIX time period. These were primarily manifested as zonal velocity oscillations u'. A prominent and critical feature was that their amplitudes of u' peaked at a variety of depths above the thermocline.

All the nine identified waves were consistent with independently observed equatorially trapped linear waves, though with different dynamical types. Generally, the waves with periods of 2–7 days are considered as inertialgravity wave. For example, Wunsch and Gill (1976) observed waves with periods of 3, 4, and 5.5 days; Luther (1980) detected a 7-day wave; Ripa and Hayes (1981) identified 2.8- and 5.3-day waves; Eriksen (1982) identified

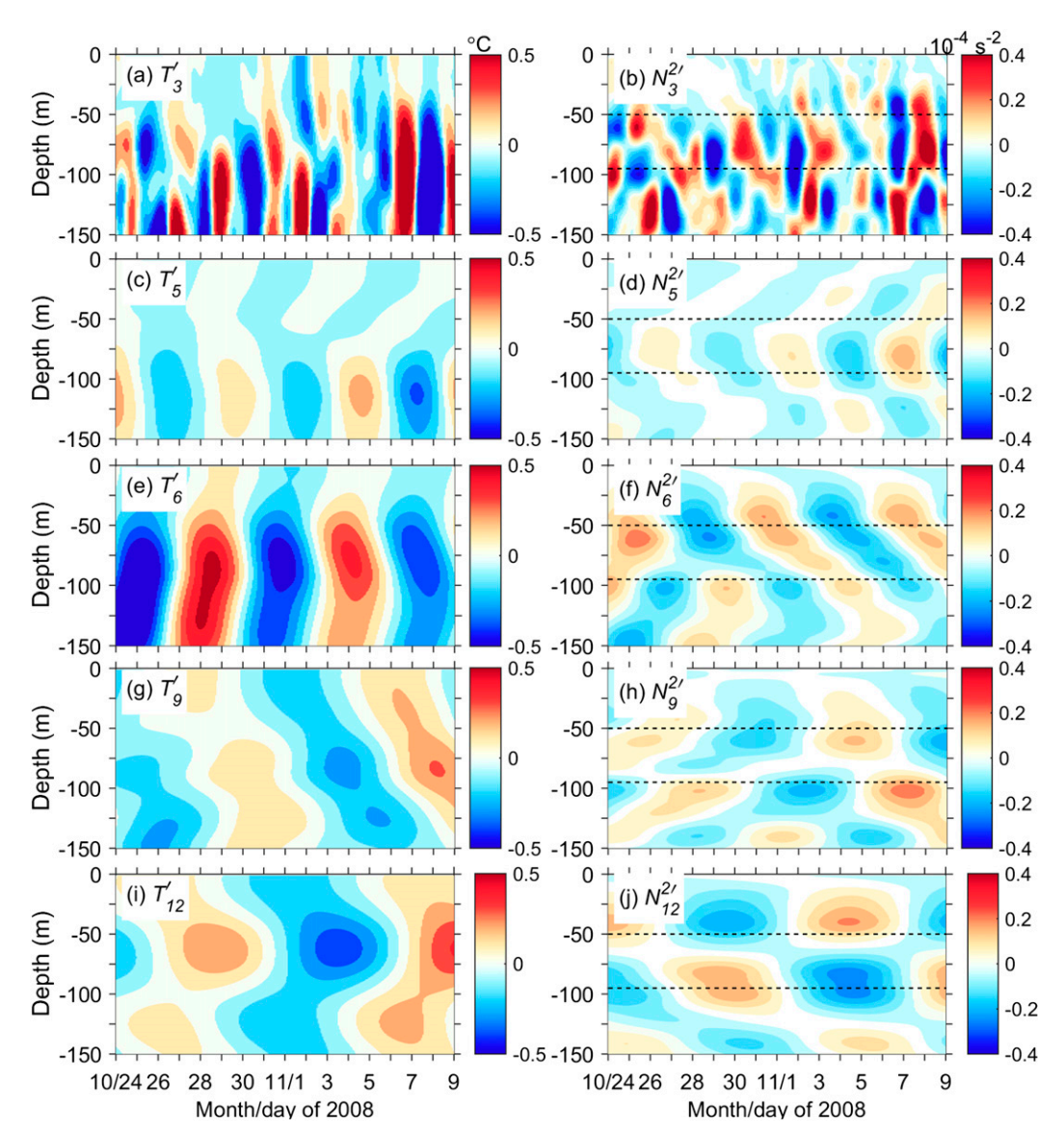


FIG. 11. (left) Temperature and (right) buoyancy frequency squared anomalies bandpass filtered at the waves' period bands for the EQUIX time period at 0°, 140°W. The two dashed lines in the left panels denote 50- and 95-m depths.

2–7-day waves; Lien et al. (1995) observed 4-day waves. Peters et al. (1991) deduced 6–16-day gravity-inertial waves from observed "shear waves." Wunsch and Gill (1976), McPhaden and Knox (1979), Luther (1980), and Eriksen (1993) provided detailed explanations of them as for (forced) equatorially trapped inertia-gravity waves. Farrar and Durland (2012) gave a systematic interpretation of the observed 2–7-day waves (and also of those 7–20-day waves) based on the dispersion relations. Furthermore, the zonal oscillating velocities on the equator are associated with the odd-numbered meridional mode of the inertial-gravity waves, which include waves with periods of ~3, ~5,

and 6–7 days, almost identical to those observed in the present study.

In the meanwhile, the waves with periods of 7–20 days are usually the Yanai wave. For example, Chiswell and Lukas (1989) observed 7–20-day waves (which they referred as 10-day waves) and considered them as Yanai wave. The frequency–wavenumber spectrum also confirms this conclusion (Farrar and Durland 2012). Particularly, W17, manifested also in v' (and primarily in v'), was the previously identified equatorial mode TIW (eTIW; Liu et al. 2019a), while W20 was the previously identified subsurface mode TIW (subTIW), which was found to grow stronger after the EQUIX time period (L19b).

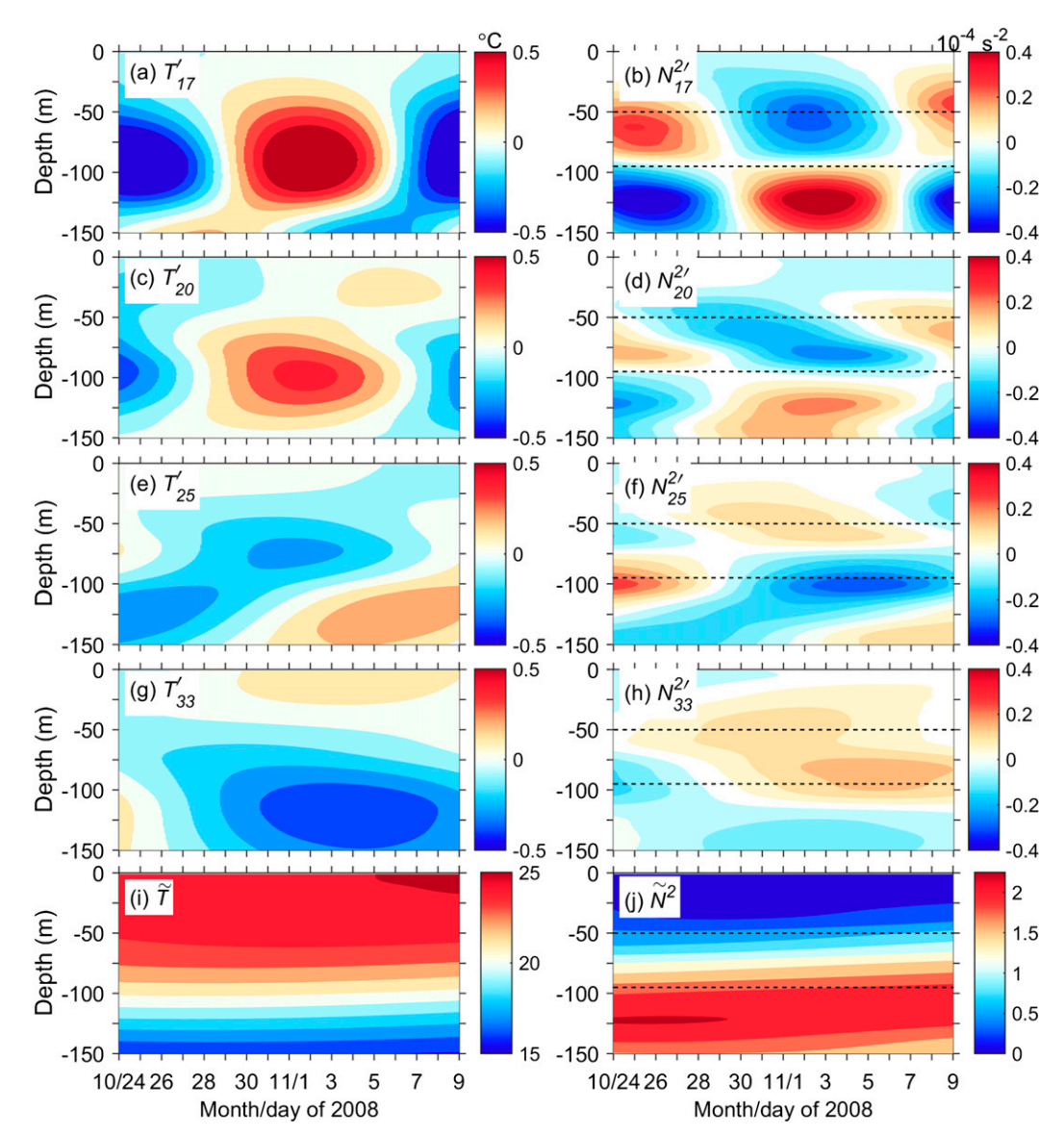


FIG. 12. (a)–(h) As in Fig. 11, but for the remainder waves, and (i)–(j) the slowly varying background temperature and buoyancy frequency squared, respectively.

Furthermore, W25 and W33 can be the well-recognized vortex mode TIW (Lyman et al. 2007; Liu et al. 2019a; Holmes and Thomas 2015; Kennan and Flament 2000). The first meridional mode of Rossby wave has zonal oscillating velocities on the equator; and the Yanai waves will also induce zonal oscillating velocities if they are in growth due to barotropic instability (Liu et al. 2019a).

As a result, the separation of the waves enables us to determine their individual contribution to the shear structures, which is crucial in forming the WSL and UCL. The increment or decrement of shear squared at different depths in the upper thermocline was primarily caused by u' of the waves, via coupling with the westward sheared

slowly varying background zonal flow; particularly, the subsurface-intensified equatorial waves resulted in out-ofphase shear squared changes (SSCs) above and below the depths of maximum amplitude of u' in the upper thermocline. In addition, in the layers just above the EUC core or the thermocline center, the meridional velocity oscillations could also occasionally induce strong positive SSCs.

The waves were also associated with different stratification anomalies which, together with the SSCs, led to the enhancement/reduction of the reduced shear and thus destabilized/stabilized the flow. First, W17 (eTIW) and W20 (subTIW) showed a $\pi/2$ phase lag of the T' (and N^2) to v', while some other subsurface-intensified

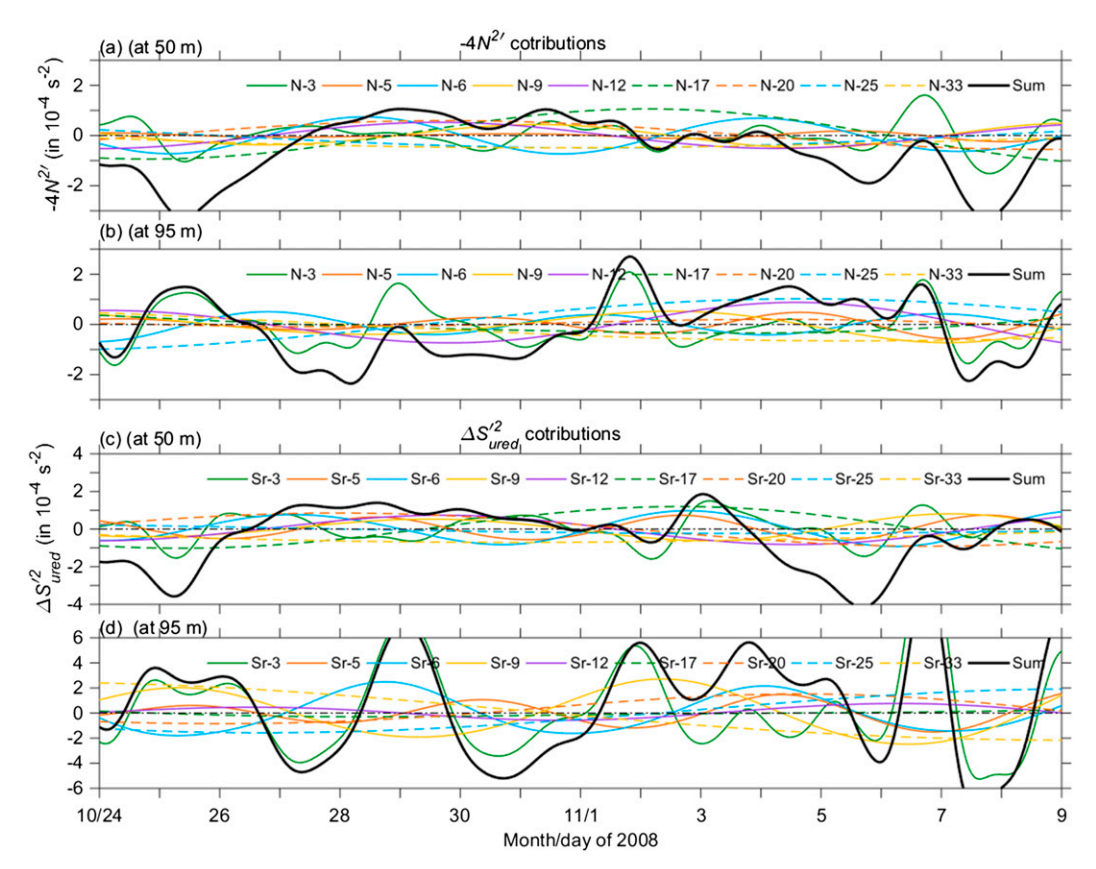


FIG. 13. (a),(b) The changes of the buoyancy frequency squared (×-4) associated with the individual waves and their sum (denoted in insets) at a WSL depth (50 m) and a UCL depth (95 m), respectively, for the EQUIX time period at 0°, 140°W. Here, "N-3" denotes $-4N_3^{2'}$, and so on. (c),(d) As in (a) and (b), but for the changes of the reduced shear squared associated with the individual waves. Here, "Sr-3" denotes $\Delta S_{u(3-3)}^{2'} + \Delta S_{u(\bar{U}-3)}^{2'} - 4N_3^{2'}$, and so on.

waves showed out-of-phase variation between T' and u'. In addition, W17 and W20 had larger vertical scale of T' and $N^{2'}$ and with the vertical phase transition layer at the thermocline center (at $\sim 100 \, \mathrm{m}$), while the other waves had small vertical scale of T' and $N^{2'}$ with varying depths as the vertical phase transition layer (varying from 65- to 85-m depths). Those features led to complexity of $N^{2'}$ and modulation of the RSSCs. However, during most of the EQUIX time period (27 October–6 November), the stratification anomalies in the upper thermocline were several factors smaller than the squared shear anomalies, and thus only played a modulating, but not controlling role, in varying the reduced shear squared. In contrast, at other times and depths, $N^{2'}$ could change $\Delta S'^2_{\rm ured}$ by amounts comparable to $\Delta S'^2_{\rm ured}$

Consequently, the reduced SS in the WSL at ~50-m depth during 3–6 November 2008 was primarily caused by W3, W5, W6, W12, and W20, while that of the UCL at ~90–100-m depth during 1–6 November 2008 was contributed occasionally by W3, W5, W6, and W20. Among them, the contribution from W6 to both the UCL and

WSL was prominent (Fig. 6). Noticeably, during the study period, a process manifested as zonal oscillation with period of \sim 70 days passed by, which greatly enhanced the SS in the UCL. In the meanwhile, the completely suppressed turbulence and mixing in the WSL were also contributed by enhanced $N^{2'}$ from W9 and W12, while the elevated turbulence and mixing in the UCL were elevated by reduced $N^{2'}$ from W12, W17, and W20.

We note that the difference in vertical resolution between the adopted velocity and temperature data did not essentially change those features—we interpolated the velocity data into the lower-resolution temperature grids and recalculated the SSCs and RSSCs, and obtained almost the same results as shown in Fig. 10. Finer structures can be expected if high-resolution temperature and salinity data were used, but can hardly change the nonturbulent WSL and turbulent UCL characteristics.

Overall, it can be concluded that the formation of either a WSL or a UCL, or a combined structure, was

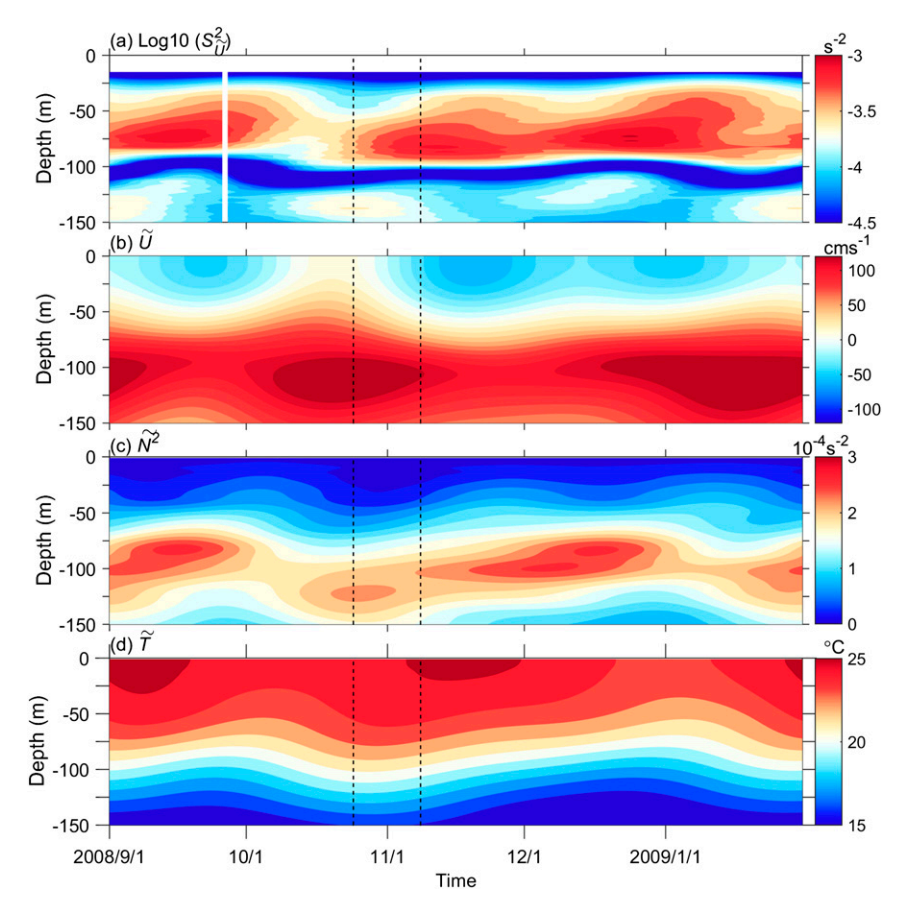


FIG. 14. The slowly varying background properties during 1 Sep 2008–31 Jan 2009 at 0°, 140°W. (a) Shear squared from the slowly varying background zonal flow; (b)–(d) the slowly varying background zonal flow, buoyancy frequency squared, and temperature, respectively. The two dashed vertical lines denote the EQUIX time period.

subject to appropriate combination of the equatorial waves, in terms not only of the depths of maximum amplitude of u' and their vertical scales and phases (in inducing appropriate shear), but also of the wave types (in inducing appropriate strain). Therefore, WSLs and UCLs could emerge, without a preference for TIW phases. The periods of the equatorial waves varied from days to 1 month, making the joint effect complex and the duration of the WSL or UCL usually short. The surface-intensified eTIW alone would not be able to induce such a complicated vertical structure; instead, subsurface-intensified waves were needed, particularly for the formation of a WSL (an extended analysis is needed to examine whether a preference of the WSL for TIW season exists).

Previous studies have focused on the effects of the surface-intensified TIWs, including the eTIWs and the vortex mode TIWs, in modulating vertical mixing in the eastern equatorial Pacific Ocean. The present work demonstrates the importance of other equatorial waves

having shorter time scales than the eTIWs and subsurface velocity peaks in resulting in local shear instability, turbulence and mixing. This work also demonstrates the importance of the eTIWs and subTIWs in modulating shear instability via stratification anomalies. In addition, due to the existence of the multiple-time-scale waves with different depths of oscillating velocity peaks, other special and complex shear and mixing structures could be expected in the upper thermocline, which should also vary with time. Those structures might result in overall enhanced mixing above the thermocline center, providing an additional mechanism for the diapycnal mixing and downward heat transfer in this region. The mixing effects, however, need to be verified and represented in those numerical models that are not able to resolve the small vertical scale of the equatorial waves. This may be crucial for a model's thermocline mixing, which can ultimately influence the mean ocean state and the variability of both the oceans and atmosphere (e.g., Meehl et al. 2001; Moum et al. 2013).

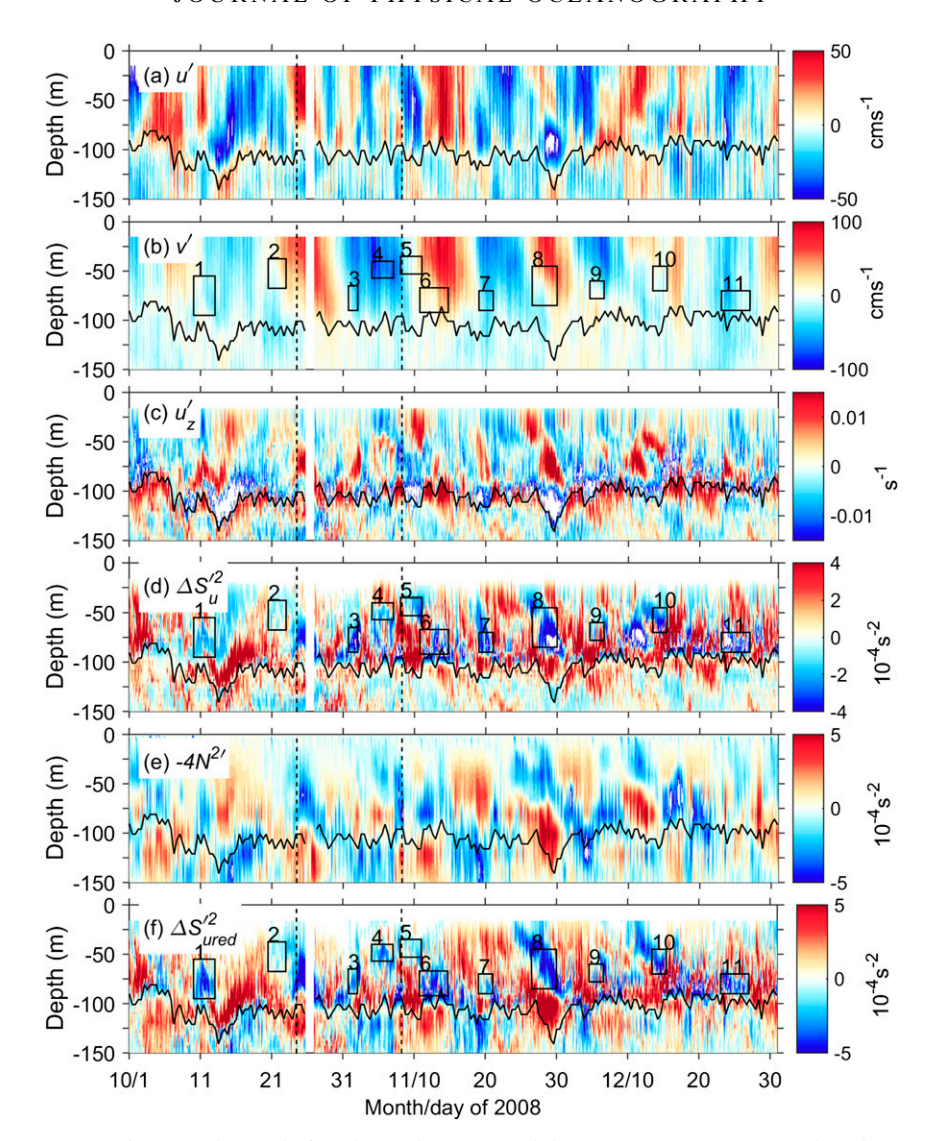


FIG. 15. Anomalous velocity, shear, shear squared, buoyancy frequency squared, and reduced shear squared, relative to their slowly varying background (defined as 45-day low-pass filtered), during 1 Oct–31 Dec 2008 at 0° , 140° W. (a),(b) The anomalous zonal and meridional velocities, respectively; (c) the anomalous shear of the zonal velocity; (d) the total shear squared changes of the zonal flow; (e) the buoyancy frequency squared changes (\times -4); and (f) the reduced shear squared changes of the zonal flow. The 11 boxes denote the detected WSLs. The black line denotes the EUC core; the two dashed vertical lines denote the EQUIX time period. Here, "anomalous" means 45-day high-pass filtered.

Efforts also need to be made in order to gain a thorough understanding of the discovered equatorial waves. One wave of particular interest might be the subsurface-intensified 6–7-day wave (W6) in terms of their generation mechanism(s) and dynamical characteristics. We note that W6 seemed to be a persistent phenomenon because it could also be detected by PSD analysis with a longer period (2000–10) and did not show seasonal preference (not shown). Wunsch and Gill (1976) observed 4–6-day sea level oscillations in the tropical

Pacific and argued that they were equatorial trapped inertial gravity waves of first baroclinic and second meridional mode forced by local wind. Owing to the zonal oscillating velocity on the equator, W6 could be a second baroclinic and first meridional inertial-gravity wave. The second physically interesting wave is the subTIW (W20). Regarding the vertical structure of the waves (including both oscillating velocity and temperature anomalies), the surface-intensified eTIWs and vortex TIWs are identified as the first baroclinic Yanai and Rossby waves,

respectively (Lyman et al. 2007; Liu et al. 2019a); analogically, the subsurface-intensified W20 was argued as the second-mode baroclinic equatorial waves. Yet, to determine their generation mechanisms and specific dynamical type, the background conditions, such as the 3D density and flow structures from numerical model outputs, must be first examined; theoretical models may also be adopted. A study using numerical model outputs may also help to identify the types of the waves and their propagation properties. In addition, the ~90-day wave displayed in the thermocline could be a Kelvin wave, yet to be verified, too. Moreover, interaction processes among the waves, particularly between the eTIW, the vortex mode TIW, and the equatorial waves (e.g., Holmes and Thomas 2016), could be important in understanding the energetics and energy cascade on the equator. Specifically, some gravity waves could be resulted from the eTIW and vortex mode TIW (Warner et al. 2018).

Acknowledgments. This study is supported by the Strategic Priority Research Program (XDA19060102, XDB42000000), the Key Research Program of Frontier Sciences (QYZDB-SSW-DQC030) of Chinese Academy of Sciences (CAS), the National Natural Science Foundation of China (41976012, Y72143101B, 41730534, 41622601 and 91858201), and the Aoshan Talents Program QNML (2017ASTCP-ES03). W.D. Smyth was funded by the U.S. National Science Foundation (OCE-1851520) and a visiting fellowship from the State Key Laboratory of Marine Environmental Science (Xiamen University). Data source (http://www.pmel.noaa.gov/tao/data_deliv) is gratefully acknowledged.

REFERENCES

- Boyd, T. J., D. S. Luther, R. A. Knox, and C. Hendershott, 1993: High frequency internal waves in the strongly sheared currents of the upper equatorial Pacific: Observations and a simple spectral model. J. Geophys. Res., 98, 18 089–18 107, https:// doi.org/10.1029/93JC01798.
- Chiswell, S. M., and R. Lukas, 1989: Rossby–gravity waves in the central equatorial Pacific Ocean during the NORPAX Hawaii-to-Tahiti shuttle experiment. J. Geophys. Res., 94, 2091–2098, https://doi.org/10.1029/JC094iC02p02091.
- Clayson, C. A., and L. H. Kantha, 1999: Turbulent kinetic energy and its dissipation rate in the equatorial mixed layer. J. Phys. Oceanogr., 29, 2146–2166, https://doi.org/10.1175/1520-0485(1999)029%3C2146:TKEAID%3E2.0.CO;2.
- Delcroix, T., J. Picaut, and G. Eldin, 1991: Equatorial kelvin and Rossby waves evidenced in the Pacific Ocean through Geosat sea level and surface current anomalies. J. Geophys. Res., 96, 3249–3262, https://doi.org/10.1029/90JC01758.
- Duchon, C. E., 1979: Lanczos filtering in one and two dimensions. J. Appl. Meteor., 18, 1016–1022, https://doi.org/10.1175/1520-0450(1979)018%3C1016:LFIOAT%3E2.0.CO;2.

- Eriksen, C. C., 1982: Equatorial wave vertical modes observed in a western Pacific island array. *J. Phys. Oceanogr.*, **12**, 1206–1227, https://doi.org/10.1175/1520-0485(1982)012%3C1206:EWVMOI%3E2.0.CO:2.
- —, 1993: Equatorial ocean response to rapidly translating wind bursts. J. Phys. Oceanogr., 23, 1208–1230, https://doi.org/ 10.1175/1520-0485(1993)023<1208:EORTRT>2.0.CO;2.
- Farrar, J. T., and T. S. Durland, 2012: Wavenumber-frequency spectra of inertia-gravity and mixed Rossby-gravity waves in the equatorial Pacific Ocean. *J. Phys. Oceanogr.*, **42**, 1859–1881, https://doi.org/10.1175/JPO-D-11-0235.1.
- Gregg, M. C., H. Peters, J. C. Wesson, N. S. Oakey, and T. J. Shay, 1985: Intensive measurements of turbulence and shear in the equatorial under current. *Nature*, 318, 140–144, https://doi.org/10.1038/318140a0.
- Holmes, R. M., and L. N. Thomas, 2015: The modulation of equatorial turbulence by tropical instability waves in a regional ocean model. *J. Phys. Oceanogr.*, 45, 1155–1173, https:// doi.org/10.1175/JPO-D-14-0209.1.
- —, and —, 2016: Modulation of tropical instability wave intensity by equatorial Kelvin waves. *J. Phys. Oceanogr.*, 46, 2623–2643, https://doi.org/10.1175/JPO-D-16-0064.1.
- Inoue, R., R. C. Lien, and J. N. Moum, 2012: Modulation of equatorial turbulence by a tropical instability wave. *J. Geophys. Res.*, 117, C10009, https://doi.org/10.1029/2011JC007767.
- Kennan, S. C., and P. J. Flament, 2000: Observations of a tropical instability vortex. J. Phys. Oceanogr., 30, 2277–2301, https:// doi.org/10.1175/1520-0485(2000)030<2277:OOATIV>2.0.CO;2.
- Lien, R.-C., D. R. Caldwell, M. C. Gregg, and J. N. Moum, 1995: Turbulence variability at the equator in the central Pacific at the beginning of the 1991-1993 El Niño. *J. Geophys. Res.*, **100**, 6881–6898, https://doi.org/10.1029/94JC03312.
- Lien, R. C., M. J. McPhaden, and M. C. Gregg, 1996: High frequency internal waves at 0°, 140°W and their possible relationship to deep cycle turbulence. J. Phys. Oceanogr., 26, 581–600, https://doi.org/ 10.1175/1520-0485(1996)026<0581:HFIWAA>2.0.CO;2.
- Liu, C., A. Köhl, Z. Liu, F. Wang, and D. Stammer, 2016: Deep-reaching thermocline mixing in the equatorial Pacific cold tongue. *Nat. Commun.*, 7, 11576, https://doi.org/10.1038/NCOMMS11576.
- ——, X. Wang, A. Köhl, F. Wang, and Z. Liu, 2019a: The northeast-southwest oscillating equatorial mode of the tropical instability wave and its impact on equatorial mixing. *Geophys. Res. Lett.*, 46, 218–225, https://doi.org/10.1029/2018GL080226.
- —, L. Fang, A. Köhl, Z. Liu, W. D. Smyth, and F. Wang, 2019b: The subsurface mode tropical instability waves in the equatorial Pacific Ocean and their impacts on shear and mixing. *Geophys. Res. Lett.*, 46, 12 270–12 278, https://doi.org/10.1029/2019GL085123.
- Luther, D. S., 1980: Observations of long period waves in the tropical ocean and atmosphere. Ph.D. thesis, Massachusetts Institute of Technology, 210 pp.
- Lyman, J. M., G. C. Johnson, and W. S. Kessler, 2007: Distinct 17and 33-day tropical instability waves in subsurface observations. J. Phys. Oceanogr., 37, 855–872, https://doi.org/10.1175/ JPO3023.1.
- Mack, A. P., and D. Hebert, 1997: Internal gravity waves in the upper eastern equatorial Pacific: Observations and numerical solution. J. Geophys. Res., 102, 21 081–21 100, https://doi.org/ 10.1029/97JC01506.
- —, and —, 1999: Mixing structure of high-frequency internal waves in the upper eastern equatorial Pacific. J. Phys. Oceanogr., 29, 3090–3100, https://doi.org/10.1175/1520-0485(1999)029%3C3090:MSOHFI%3E2.0.CO;2.

- McPhaden, M. J., 1995: The Tropical Atmosphere Ocean array is completed. *Bull. Amer. Meteor. Soc.*, **76**, 739–744, https://doi.org/10.1175/1520-0477-76.5.739.
- ——, and R. A. Knox, 1979: Equatorial kelvin and inertio-gravity waves in a zonal shear flow. J. Phys. Oceanogr., 9, 263–277, https:// doi.org/10.1175/1520-0485(1979)009<0263:EKAIGW>2.0.CO;2.
- —, and H. Peters, 1992: Diurnal cycle of internal wave variation in the equatorial Pacific Ocean: Results from moored observations. J. Phys. Oceanogr., 22, 1317–1329, https://doi.org/10.1175/ 1520-0485(1992)022%3C1317:DCOIWV%3E2.0.CO;2.
- Meehl, G. A., P. R. Gent, J. M. Arblaster, B. L. Otto-Bliesner, E. C. Brady, and A. Craig, 2001: Factors that affect the amplitude of El Niño in global coupled climate models. *Climate Dyn.*, 17, 515–526, https://doi.org/10.1007/PL00007929.
- Moum, J. N., and D. R. Caldwell, 1985: Local influences on shear flow turbulence in the equatorial ocean. *Science*, 230, 315–316, https://doi.org/10.1126/science.230.4723.315.
- —, D. Hebert, C. A. Paulson, and D. R. Caldwell, 1992: Turbulence and internal waves at the equator. Part I: Statistics from towed thermistors and a microstructure profiler. *J. Phys. Oceanogr.*, 22, 1330–1345, https://doi.org/10.1175/1520-0485(1992)022<1330:TAIWAT>2.0.CO;2.
- ——, R. C. Lien, A. Perlin, J. D. Nash, M. C. Gregg, and P. J. Wiles, 2009: Sea surface cooling at the equator by subsurface mixing in tropical instability waves. *Nat. Geosci.*, 2, 761–765, https:// doi.org/10.1038/ngeo657.
- —, J. D. Nash, and W. D. Smyth, 2011: Narrowband oscillations in the upper equatorial ocean. Part I: Interpretation as shear instabilities. *J. Phys. Oceanogr.*, 41, 397–411, https://doi.org/ 10.1175/2010JPO4450.1.
- —, A. Perlin, J. D. Nash, and M. J. McPhaden, 2013: Seasonal sea surface cooling in the equatorial Pacific cold tongue controlled by ocean mixing. *Nature*, 500, 64–67, https://doi.org/10.1038/ nature12363.
- Peters, H., M. C. Gregg, and T. B. Sanford, 1991: Equatorial and off-equatorial fine-scale and large-scale shear variability at 140°W.
 J. Geophys. Res., 96, 16913–16928, https://doi.org/10.1029/91JC01317.
- —, —, and —, 1994: The diurnal cycle of the upper equatorial ocean: Turbulence, fine-scale shear, and mean shear.
 J. Geophys. Res., 99, 7707–7723, https://doi.org/10.1029/93JC03506.
- Pham, H., W. D. Smyth, S. Sarkar, and J. N. Moum, 2017: Seasonality of deep cycle turbulence in the eastern equatorial Pacific. J. Phys. Oceanogr., 47, 2189–2209, https://doi.org/ 10.1175/JPO-D-17-0008.1.
- ——, S. Sarkar, and K. B. Winters, 2013: Large-eddy simulation of deep-cycle turbulence in an equatorial undercurrent model. *J. Phys. Oceanogr.*, 43, 2490–2502, https://doi.org/10.1175/ JPO-D-13-016.1.
- Ripa, P., and S. P. Hayes, 1981: Evidence for equatorial trapped waves at the Gala'pagos Islands. *J. Geophys. Res.*, **86**, 6509–6516, https://doi.org/10.1029/JC086iC07p06509.

- Schudlich, R. R., and J. F. Price, 1992: Diurnal cycles of current, temperature, and turbulent dissipation in a model of the equatorial upper ocean. J. Geophys. Res., 97, 5409–5422, https://doi.org/10.1029/91JC01918.
- Skyllingstad, E. D., and D. W. Denbo, 1994: The role of internal gravity waves in the equatorial current system. *J. Phys. Oceanogr.*, 24, 2093–2110, https://doi.org/10.1175/1520-0485(1994)024<2093: TROIGW>2.0.CO;2.
- Smyth, W. D., and J. N. Moum, 2002: Shear instability and gravity wave saturation in an asymmetrically stratified jet. *Dyn. Atmos. Oceans*, 35, 265–294, https://doi.org/10.1016/S0377-0265(02)00013-1.
- —, and —, 2013: Marginal instability and deep cycle turbulence in the eastern equatorial Pacific Ocean. *Geophys. Res. Lett.*, 40, 6181–6185, https://doi.org/10.1002/2013GL058403.
- —, —, L. Li, and S. A. Thorpe, 2013: Diurnal shear instability, the descent of the surface shear layer, and the deep cycle of equatorial turbulence. *J. Phys. Oceanogr.*, 43, 2432–2455, https://doi.org/10.1175/JPO-D-13-089.1.
- —, H. Pham, J. N. Moum, and S. Sarkar, 2017: Pulsating turbulence in a marginally unstable stratified shear flow. *J. Fluid Mech.*, **822**, 327–341, https://doi.org/10.1017/jfm.2017.283.
- Sun, C., W. D. Smyth, and J. N. Moum, 1998: Dynamic instability of stratified shear flow in the upper equatorial Pacific. *J. Geophys. Res.*, 103, 10 323–10 337, https://doi.org/10.1029/98JC00191.
- Sutherland, B. R., 1996: Dynamic excitation of internal gravity waves in the equatorial oceans. *J. Phys. Oceanogr.*, **26**, 2398–2419, https://doi.org/10.1175/1520-0485(1996)026<2398:DEOIGW>2.0.CO;2.
- Wang, D., and P. Müller, 2002: Effects of equatorial undercurrent shear on upper ocean mixing and internal waves. J. Phys. Oceanogr., 32, 1041–1057, https://doi.org/10.1175/1520-0485(2002)032<1041:EOEUSO>2.0.CO;2.
- —, J. C. McWilliams, and W. G. Large, 1998: Large-eddy simulation of the diurnal cycle of deep equatorial turbulence. J. Phys. Oceanogr., 28, 129–148, https://doi.org/10.1175/1520-0485(1998)028<0129:LESOTD>2.0.CO;2.
- Wang, W., and M. J. McPhaden, 1999: The surface-layer heat balance in the equatorial Pacific Ocean. Part I: Mean seasonal cycle, J. Phys. Oceanogr., 29, 1812–1831, https://doi.org/10.1175/1520-0485(1999)029%3C1812:TSLHBI%3E2.0.CO;2.
- —, and —, 2001: What is the mean seasonal cycle of surface heat flux in the equatorial Pacific? *J. Geophys. Res.*, **106**, 837– 857, https://doi.org/10.1029/1999JC000076.
- Warner, S. J., R. M. Holmes, E. H. Hawkins, M. S. Hoecker-Martínez, A. C. Savage, and J. N. Moum, 2018: Buoyant gravity currents released from tropical instability waves. *J. Phys. Oceanogr.*, 48, 361–382, https://doi.org/10.1175/JPO-D-17-0144.1.
- Wijesekera, H. W., and T. M. Dillon, 1991: Internal waves and mixing in the upper equatorial Pacific Ocean. *J. Geophys. Res.*, **96**, 7115–7125, https://doi.org/10.1029/90JC02727.
- Wunsch, C., and A. E. Gill, 1976: Observations of equatorially trapped waves in Pacific sea level variations. *Deep-Sea Res. Oceanogr. Abstr.*, 23, 371–390, https://doi.org/10.1016/0011-7471(76)90835-4.